Des exemples de détecteurs : Detector systems in ultra relativistic heavy ion collisions

E. Nappi

Detector systems in ultra relativistic heavy ion collisions

Eugenio Nappi
INFN – Sezione di Bari, 70124 Bari, Italy

Résumé: Les collisions d'ions lourds ultra relativistes peuvent fournir les conditions extrêmes de haute densité d'énergie permettant de produire la transition à un état de vie courte appelé Plasma de Quarks et de Gluons (PQG) dans lequel les quarks ne sont plus confinés à l'intérieur des nucléons.
Après de nombreuses études au SPS du CERN, une nouvelle génération d'installations spécialisées fournira des densités d'énergie initiales encore plus élevées grâce à des collisions de faisceaux de noyaux lourds à des énergies sans précédent : le collisionneur d'ions lourds relativistes (RHIC) mis en service à BNL en 2000 et le futur grand collisionneur de hadrons (LHC) au CERN prévu pour 2006.
Quatre nouvelles expériences avec des caractéristiques complémentaires ont déjà commencé à prendre des données à RHIC, alors qu'ALICE (A Large Ion Collider Experiment), le seul détecteur dédie à ce type de physique au LHC, est en ce moment en construction.
Le but de ce cours est de faire la revue des concepts des techniques expérimentales envisagées. Les différents sous-systèmes seront illustrés en détails en insistant sur les solutions expérimentales choisies pour étudier au mieux les signatures subtiles de la formation du PQG.

Abstract: Ultra-relativistic heavy ion collisions are believed to provide the extreme conditions of energy densities able to determine the transition to a short-lived state, called Quark-Gluon Plasma (QGP), where the quarks are no longer confined within the dimensions of the nucleons.
After many years of studies at CERN-SPS, a new generation of dedicated facilities will provide higher initial densities by colliding heavy nuclei head-on at unprecedented energies: the Relativistic Heavy Ion Collider (RHIC), commissioned at BNL in 2000, and the forthcoming Large Hadron Collider (LHC) at CERN, due to start in 2006.
Four novel experiments, with complementary features, have already started to take data at RHIC, while ALICE (A Large Ion Collider Experiment), the only dedicated experiment for heavy ion collision at LHC, is presently under construction.
The aim of this course is to overview the techniques envisaged in the experiment layouts. The various sub-systems will be illustrated in detail with emphasis on the experimental solutions adopted to investigate the challenging signatures of the QGP formation. The overview will be preceded by an introduction describing the underlying physics goals.

1. INTRODUCTION

According to the current theory of the strong interactions, Quantum Chromo-Dynamics (QCD), spin-½ quarks are the elementary constituents of hadronic matter and they interact by exchanging massless vector fields, called gluons, coupled to the matter fields through a set of three "colour" charges (the concept of quark carrying a "colour" charge led to the name QCD).

Although QCD was formulated by analogy with Quantum Electro-Dynamics (QED) where the role of gluons is played by photons, carriers of the electromagnetic interaction, a profound difference exists between the two theories: gluons are directly coupled among themselves, unlike the photons which are electrically neutral and therefore can couple only through electron loops.

One of the consequences of the direct coupling among gluons is that the field between two colour sources is limited to a thin string about 1 fm (10^{-15} m) across, with a resulting effective potential increasing linearly with r (the string tension). This peculiar behaviour, called "colour confinement", entails that the strong interaction remains constant as the sources move apart whereas in the case of electrical charges the field falls off at large distances.

The colour confinement is the most evident manifestation of the complicated structure of the QCD vacuum that, acting as a "colour" dielectric, prevents the strong field to extend away from any set of colour sources (see Section 2.1). Consequently hadrons are a globally neutral system with respect to colours (colour singlets). Combination of three quarks(*) carrying each a different colour makes up colourless non-integer spin hadrons, called baryons. Integer spin hadrons (mesons) are instead made up of combinations of a quark of a certain colour and an antiquark with the corresponding anti-colour.

Both quarks and gluons cannot be observed outside the hadrons; in fact by attempting to pull apart from each other two quarks, the interaction energy would increase up to a point where new quark pairs are created from the vacuum thus neutralizing the colour of the previous quarks and forming new colour neutral objects (hadronization mechanism).

Whilst any QED phenomenon can be calculated in a perturbative way, such an approach is applicable in QCD only to the strong interaction processes at large momentum transfer (or equivalently at short distance) where quarks and gluons appear to be weakly coupled due to the logarithmic decrease of the interaction strength between two coloured objects as they get closer (asymptotic freedom).

(*) Six varieties of quarks, called "flavors", can account for the properties of the entire multitude of hadrons. Flavors are labelled u (up), c (charm), t (top), d (down), s (strange) and b (bottom).

For distances approaching the typical hadron size (~fm), the effective coupling constant is larger than one owing to the QCD vacuum structure, thus requiring a non-perturbative approach. In fact, perturbation theory to any finite order in QCD depicts only a particle spectrum made of quarks and gluons in contrast to the confinement property.
A very promising non-perturbative technique is lattice-QCD: a Monte Carlo simulation that approximates the continuous space-time of real world into a discrete lattice.
Good statistics for accurate predictions on large lattices, with a grid spacing rather small to capture any details in the structure of the quantum field, require the employment of a huge computer power and a long running time. Nevertheless, computations with three dynamical light quark flavors on the lattice [1] revealed interesting insights into the behaviour of hadronic matter under extreme conditions of density and indicated that a phase transition from hadronic gas to QGP is expected at low quark chemical potential and at a temperature (*) of T_c~ 170 MeV which corresponds to an energy density ε_c=0.6 GeV/fm^3 (Fig.1).

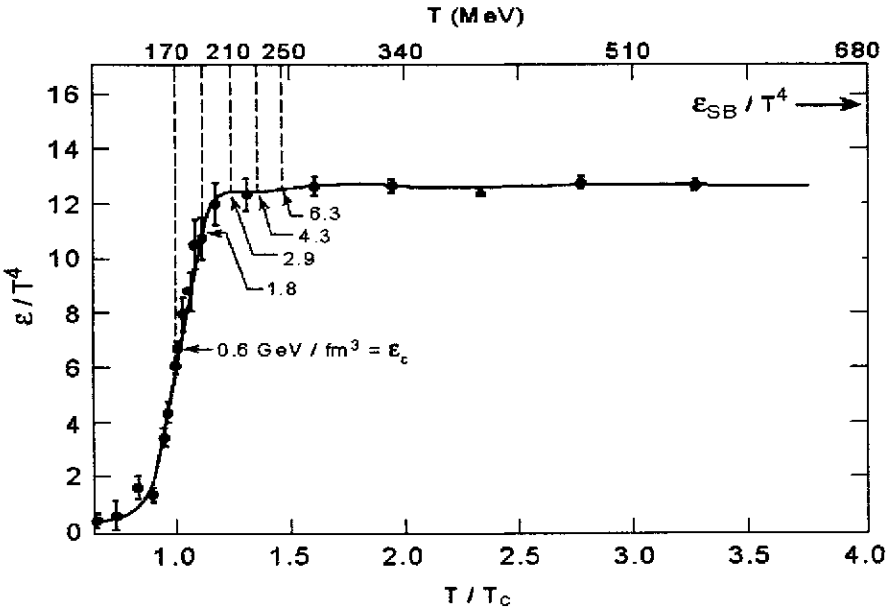

Fig.1. Lattice-QCD calculations of the energy density plotted in units of T^4; ε_{SB} is the energy density of an ideal Stefan-Boltzmann gas system of non-interacting quarks and gluons.

(*) Temperature is defined by the relationship: kT= average kinetic energy per nucleon (k is the Boltzmann constant of proportionality: 1 MeV ~ 1.2 x 10^{10} K).
T_C (QGP) ~ 170 MeV ~ 2040 10^9 K (much more than the temperature of supernova, the hottest process active nowadays in the Universe)

This paper consists of five parts: after an introduction on the underlying physics concepts, the main observables and signatures investigated in the study of ultrarelativistic heavy ion collisions are described in the framework of the results already achieved at CERN-SPS. The successive parts are devoted to the research programmes planned at the novel facilities (RHIC and LHC) and to the related experimental issues. Finally, an in-depth description of the ALICE experiment at LHC is provided.
The present paper is not meant to cover all the aspects of the investigation of the phase transition of hadronic matter to the QGP but rather to provide some context of the field. Interested readers are referred to the excellent books of Hwa[2] and the manuscripts of Kuhn [3] and Harris [4].

2. The Quark-Gluon Plasma

At the light of lattice-QCD predictions, the diagram for expected new phases of nuclear matter is shown in Fig.2.

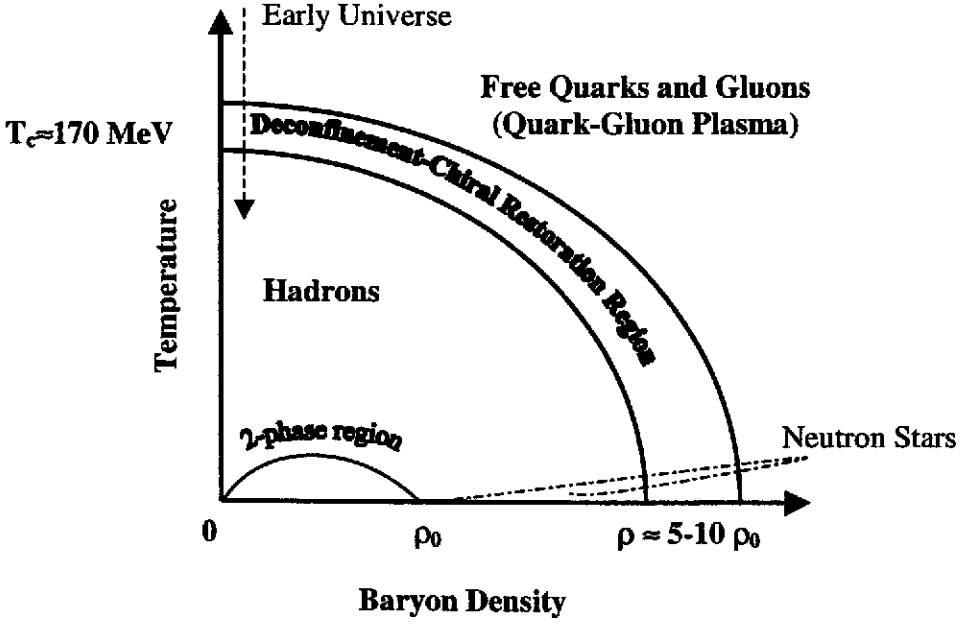

Fig.2. Phase diagram of nuclear matter showing regions of hadronic and deconfined matter. Ordinary nuclear matter density is ρ_0=0.14 nucleons · fm^{-3}.

Whilst in the low temperature and baryon density region, the basic degrees of freedom are hadronic (nucleons, mesons...), at high temperature and baryon density the basic degrees of freedom become those of quarks and gluons.

QGP would not be a mere "lab-creation" but it is supposed to be the primordial soup that originated the hadronic matter after the Big Bang, in the process of hadro-synthesis, as shown in Fig.3. The matter of the early Universe had a relatively small net baryon density, as the universe expanded it cooled and matter hadronized, following a downward trajectory practically along the vertical axis of the phase diagram.
A dense state of matter is thought to exist also in the interior of neutron stars [5]. The very high pressure of the core of a neutron star could in fact lead to the formation of a QGP.

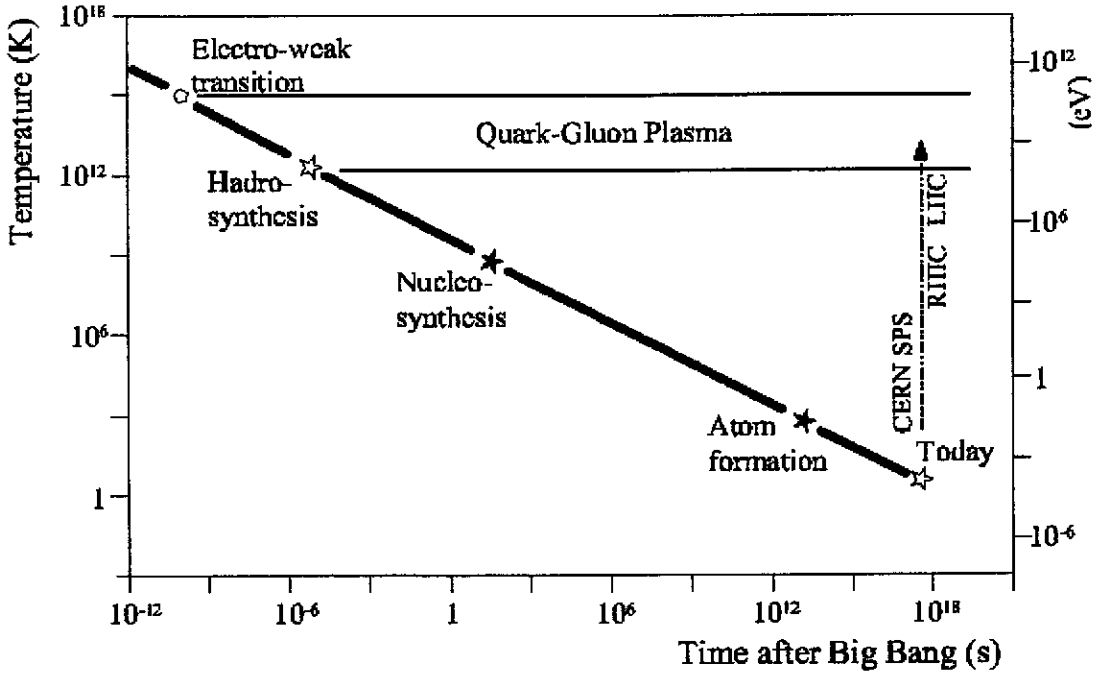

Fig.3. The transition from the primordial plasma of quarks and gluons to ordinary matter occurred some 10^{-5} s after Big Bang when the temperature lowered to about 10^{12} K. The inverse process is expected to occur nowadays at RHIC (and in near future at LHC).

The study of the properties of dense matter at low temperature would allow not only to achieve a more accurate knowledge of the dynamics of the evolution of neutron stars in supernovae, as a consequence of the huge compression of matter by gravitational collapse, but also to evaluate with better accuracy the correlation between the stability of neutron stars and their maximum mass.
Finally, the study of strongly interacting matter under extreme conditions of high energy density, beyond its paramount importance of addressing a new phase of matter and the above-mentioned exciting issues in astrophysics and

cosmology, is expected to reveal key insights into the fundamental questions of confinement and broken chiral symmetry. In fact, in the framework of statistical QCD, the phase transition from the ordinary nuclear matter to the QGP is accompanied by chiral symmetry restoration resulting in modified nuclear states and excitation of vacuum.

2.1 The QCD-vacuum and the chiral symmetry

According to the field theories, the phenomenon of quantum fluctuations led to a revision of the concept of vacuum being it no more an empty space as in the classical idea but a complex entity filled by virtual particle-antiparticle pairs. However, the resulting effect of vacuum polarization has a completely different behaviour in QED with respect to QCD, because in the latter theory the polarization from quark-antiquark pairs is not sufficient to offset the effect of interaction with the virtual gluons filling the vacuum.
Hence, the property of gluons to carry colour charge entails the remarkable effect of "anti-screening" of pair creation oppositely to the screening effect of pair creation in the QED vacuum.
Hadrons can therefore be imaged as bubbles within the "anti-screening" vacuum that behaves as a liquid, i.e. as small regions of space where the colour flux tubes between the constituent quarks are severely confined, the whole system having neutral colour. Such a behaviour inspired the "Bag model" in which quarks and gluons modify the vacuum in their vicinity, carving out regions of perturbative vacuum (bags) immersed in the normal non-perturbative vacuum: quarks and gluons propagate freely in the bags, but are strongly repelled by the non-perturbative vacuum. The bag constant B measures the excess energy density of the perturbative vacuum, and hence is a measure of the pressure of the normal vacuum on the bubble of perturbative vacuum.
The states of virtual excitations that dress quarks with dense gluon and quark-antiquark clouds modify the value of the quark mass depending on the distance at which the mass is measured: the shorter the distance, the smaller the mass is.
The two following extreme cases are particularly relevant:

- at very short distances (of the order of 10^{-14} cm), gluon influence is negligible owing to the asymptotic freedom: the mass of light quarks u and d is close to zero (m_u~5 MeV/c^2 and m_d~7 MeV/c^2). Quarks are called "current quarks";
- at large distances, quarks acquire a large effective mass via interactions between themselves and the surrounding gluon clouds.

The largest mass value for u and d quarks is about 300 MeV/c^2, i.e. 1/3 of the nucleon mass by assuming that the mass of a nucleon is the sum of the masses of the three non-relativistic constituent quarks.
The QCD Lagrangian with massless u and d quarks reflects the existence of an underlying chiral symmetry since it consists of two components related to the splitting into two "handedness" terms. This is a consequence of the fact that massless particles possess a specific conserved helicity (the projection of the spin of a particle on its momentum) defined as left-handed (L) if the directions of spin and momentum are opposite and as right-handed (R) if they are identically oriented.
Helicity cannot be defined in a Lorentz-invariant manner for particles with nonzero mass, for istance a right-handed electron can be converted into a left-handed by changing the reference frame. On the contrary, massless particles move at the speed of light and hence there is no observer travelling faster to reverse the direction of motion and therefore the helicity of massless particles is Lorentz-invariant. This is similar to the case of real photons that can have only two transverse polarizations.
Emission and absorption of vector gluons by colour charges of quarks do not change quark helicities: the QCD Lagrangian of massless quarks naturally factorizes into two symmetric terms, one of which contains left-handed quarks u_L,d_L and the other, right-handed quarks u_R,d_R; left-handed quarks interact only with left-handed antiquarks and similarly for the right-handed ones. Hence, although the Lagrangian has a definite symmetry, the physical states (nonzero mass nucleons) do not have it, with the net result that chiral symmetry is spontaneously broken through the creation of a vacuum scalar condensate (left-handed quarks and right-handed antiquarks and viceversa) that couples to the hadrons thus providing most of their mass.
As the QGP phase occurs, the chiral symmetry is expected to be restored (or partially restored) since the new degrees of freedom are (almost) massless quarks and gluons acting as free particles.

3. Ultra-relativistic nuclear collisions

As shown in the phase diagram of matter (Fig.2), ordinary nuclei are located in a region defined by a temperature much smaller than the proton and pion

rest masses and a baryon density(*) of about 0.14 nucleons/fm^3 corresponding to an energy density of 130 MeV/fm^3 (ρ=2.3 10^{14} g/cm^3).
This means that distances between nucleons are larger than their radius ($\approx$0.8 fm), whereas the transformation of ordinary matter into QGP requires that the nucleon wave functions significantly overlap each other, condition likely reachable by smashing together, at relativistic energies, heavy nuclei that thus become very hot and very dense as a consequence of the substantial squeezing occurring in the collision.
An energy density many times higher than that of ordinary nuclear matter will be achieved in this way and hence nucleons will lose their identity by melting into a soup of quarks and gluons through a process that reverses the early Universe history.
As it will be described in Sect. 3.2, from an experimental point of view, the most convenient way to study QGP complicated behaviour is to produce a high energy density system in thermal equilibrium with a rather long lifetime. This entails that the deconfinement of quarks and gluons must preferably occur over a sufficiently large volume, compared to their scattering length, and hence in interactions between extended hadronic objects as heavy nuclei. The several rescattering processes experienced by the produced particles will redistribute the available centre of mass energy in higher degrees of freedom thus producing a state of thermal equilibrium.
On the contrary, although the energy densities achieved in collision e+e- or pp could be as high as in colliding heavy nuclei, tiny projectiles as leptons and nucleons are unable to create QGP since the overall size of the interaction region would be too small to study the effects of deconfinement.
Moreover, because of the rather short range of the strong interactions and the subsequent evolution of the QGP, the relevant experimental observables come mainly from the interior of the dense energy region whilst background is essentially originated on the surface. Consequently the signal over background ratio is proportional to the colliding object's volume over surface ratio thus favouring, also in this case, the employment of heavy nuclei (Sect. 3.2).

(*)For a nucleus of atomic mass A and radius R~1.2A$^{1/3}$ fm, the density of nucleons ρ_0 is almost constant (no dependence from A):

$$\rho_0 = \frac{\text{A nucleons}}{\frac{4}{3}\pi R^3} \cong 0.14 \frac{\text{nucleons}}{\text{fm}^3}$$

3.1 Space-time evolution of nuclear collisions

Scattering reactions between heavy nuclei are characterized by the number of participant and spectator nucleons. A simple geometrical description, based on the impact parameter b, is indeed possible owing to the relevant size of heavy nuclei whose radius is larger than the interaction length: only some nucleons of both nuclei do participate in the interaction and therefore are called "participants" while the others, not in geometrical overlap with each other, remain as "spectators" (Fig. 4).
Central collision events (b~0) are the best candidate for searching QGP because grazing or peripheral collisions at large b do not provide the geometrical overlap of enough nucleons mandatory to achieve a high energy density in a large volume.

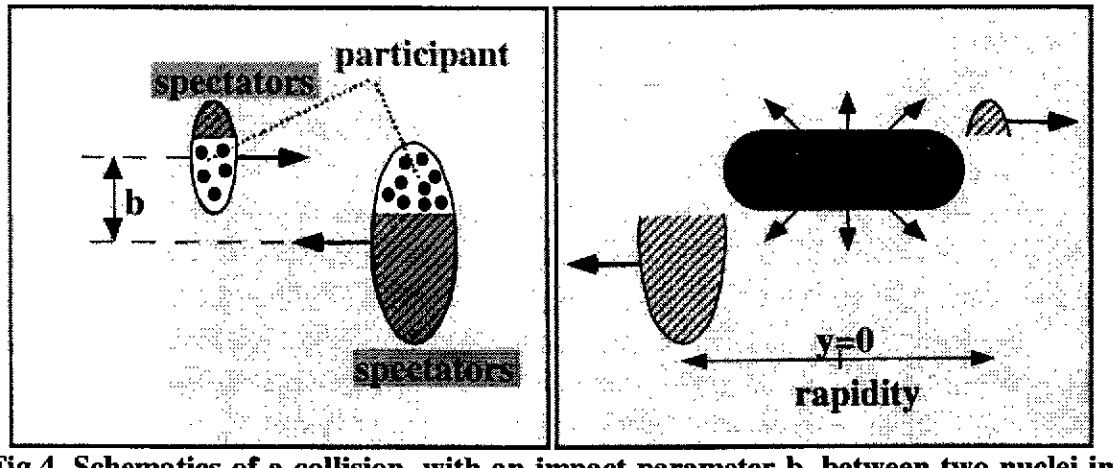

Fig.4. Schematics of a collision, with an impact parameter b, between two nuclei in the centre-of-mass system. The hot volume created by the participants consists of two regions: the central region (centred at y=0) almost baryon-free at the energy regimes of RHIC and LHC and the fragmentation region (at high rapidity) rich in nucleons.

The theoretical interpretation of the space-time evolution of a collision between two nuclei at very high energies is based on the assumption that, as soon as the nucleons penetrate through each other, quarks and gluons experience hard scatterings. The kinetic energy of the incoming nuclei is transferred from the longitudinal into the accessible transverse degrees of freedom.
After the "formation time" (about 1 fm/c), quarks and gluons materialize out of the highly excited colour field and thermal equilibrium is approached via reaction between individual pairs leading to the creation of the so-called "fireball". At this point the system expands rapidly, mainly along the

longitudinal direction, and cools down thus reaching the transition temperature T_c for the creation of QGP.
In the subsequent mixed phase, hadronization starts in the "fireball" that still expands, likely in an ordered motion (large outward flow) through a hadron gas phase (Fig.5) until the "freeze out" is achieved when interactions cease and particles freely leave the reaction region and eventually can be detected by the experimental instrumentation. Each phase has associated specific signals that can be observed by experiments as it will be illustrated in the next section (Sect.3.2).

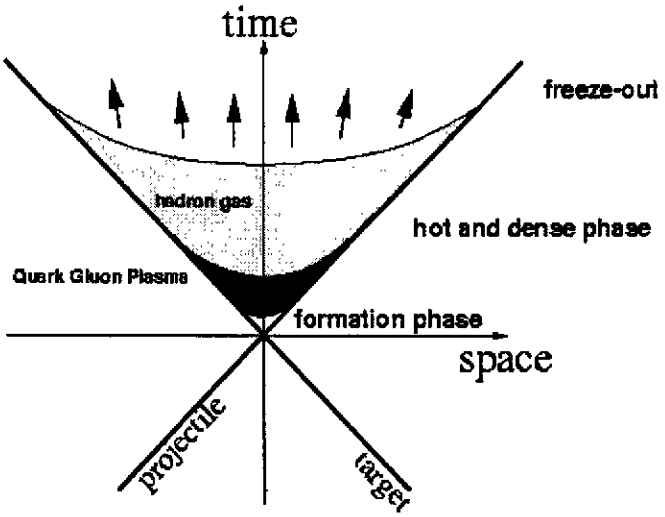

Fig.5. Space-time diagram of the evolution of an ultra-relativistic nuclear collision as viewed in the nucleon-nucleon centre-of-mass system.

Ultrarelativistic nuclear collisions are conveniently described in the rapidity(*) variable: the baryons appear in the centre of mass frame, predominantly at the rapidities of the initial beams, while in the central rapidity region one expects the bulk of created particles.
As already mentioned, according to theoretical predictions, QGP may occur at about 0.6 GeV/fm^3 (which is about 5 times the nucleus density).

(*) Rapidity is a Lorentz-invariant longitudinal "velocity" defined by

$$y = \frac{1}{2}\ln\frac{E+p_L}{E-p_L} = \tanh^{-1}\left(\frac{p_L}{E}\right)$$

where E is the particle's energy and p_L is its longitudinal momentum parallel to the beam. In the case of transverse momentum $p_T=0$ and $p_l/E=\beta<<1$, $y\approx\beta$ (particle velocity). It is an additive quantity under Lorentz transformation along the beam axis (the shape of distributions in this variable is invariant under a Lorentz transformation): passing from the center-of-mass system (cms) to the laboratory system (ls) the rapidity distribution is the same, with the y-scale displaced by an amount equal to y_{cm}.

The attained energy density ε, defined as the amount of the energy made available in the collision divided by the volume of the interaction region, is experimentally estimated from the following equation based on Bjorken's model [6]:

$$\varepsilon = \frac{\text{particle's average energy x number of particles}}{\text{interaction volume}} = \frac{1}{c\tau_0 \pi r_0^2 A_p^{2/3}} \frac{dE_T}{dy}$$

Here τ_0 is the formation time of the QGP state (typically ~1 fm/c) and $r_0 A_p^{1/3}$ is the projectile's nuclear radius. The transverse energy, E_T, is the energy lost by the incident baryons that is redistributed among many particles emitted at polar angles θ_i. It is defined as

$$E_T = \sum_i E_i \sin\theta_i$$

where E_i is the kinetic energy for baryons and the total energy for all other particles. The highest transverse energies correspond to the most violent central collisions where the conditions to create the QGP are more likely to develop.

3.2 Experimental probes and QGP's signatures

The main difficulty in hunting the QGP arises from the fact that once formed, it blows away almost immediately as the high-density nuclear matter expands, cools down and hadronizes.
Ideally QGP is similar to a black-body and in principle it is expected to obey the equation of Stefan-Boltzmann law for a system of non-interacting particles ($\varepsilon \propto T^4$) and hence, the entire hot volume of the interaction region will likely radiate a large number of photons and lepton pairs at low invariant mass. Oppositely, pions will be emitted mainly from the surface at lower temperature than photons and they will cease to interact when the density has fallen enough ("freeze-out" phase). In a few 10^{-23} s, most of the particles undergo significant reinteractions between the time of their production and their final detection. Consequently QGP's transient existence must be inferred from what remains once everything interesting has already happened thus making the "direct" identification of the QGP quite a hard task.
The current experimental approach aims at identifying observables that either decouple at different times from the expansion or are more sensitive to the early and hot stages of matter. Moreover, since theorists are not yet able

to define any single definitive signature for the QGP, many experimental observables must be measured to test unambiguously the plasma formation. The application of this strategy in the experiments performed for several years at CERN-SPS, formerly with oxygen and sulphur and later with lead nuclei, at the relatively low energy of 18-20 GeV in the nucleon-nucleon centre-of-mass, allowed to achieve a multitude of crucial results consistent with the hypothesis that a new phase of the QCD matter has been indeed created. Evidence for the onset of new collective phenomena has been also proved and the initial, dense hadronic medium (right after hadronization) has already revealed, at SPS-energies, a microscopic makeup characteristic of the conditions predicted by QCD chiral symmetry restoration, thus sheding first light on the suspected coincidence of the deconfinement and chiral restoration QCD transition. However, data are not providing unambiguous proof but each of them support different facets of the consequences expected to arise from a transient bulk deconfined QCD state formed early in the reaction dynamics of heavy nucleus collisions.
In the following sections, the most significative QGP's signatures will be reviewed in the light of the great outcomes from SPS runs, which motivated the present enthusiasm in the field.

3.2.1 Global observables: density of energy and temperature

According to the Bjorken model, events in which QGP has been achieved are likely characterized by the presence of a large amount of transverse energy and secondary particles and hence by a large amount of energy deposited during the collision. Experimental estimates from calorimetric study of bulk transverse energy production and from hadron yield measurement in full phase space indicate that the theoretical density has been already reached in sulphur induced reactions, and far surpassed in central Pb+Pb collisions [7,8]. In fact, from the value measured at NA49, one calculates an energy density of the order of 2-3 GeV/fm^3 in central collisions [7], well above the critical energy density evaluated via lattice-QCD simulations.
Another valuable tool for understanding hadronic reaction is the measurement of inclusive transverse momentum distribution. This is certainly true even in the study of heavy ion collisions where a dramatic increase of $\langle p_t \rangle$ could be the signal of the phase transition from ordinary matter to QGP.
A comparison of particle spectra at high p_T allows to disentangle possible phase transition effects from nuclear or hadronic medium effects; in fact,

large differences in the high p_t tails of spectra are predicted depending upon various medium effects.
Data are properly plotted against the transverse mass, $m_T=(p_T^2+m^2)^{1/2}$, rather than p_T, being the slope of such distributions proportional to the inverse of the temperature T in the truly thermal case(*).
SPS data [9] provided first glimpses at the non-perturbative QCD mechanism by showing temperatures in agreement with Monte Carlo lattice predictions as can be seen in Fig.6.

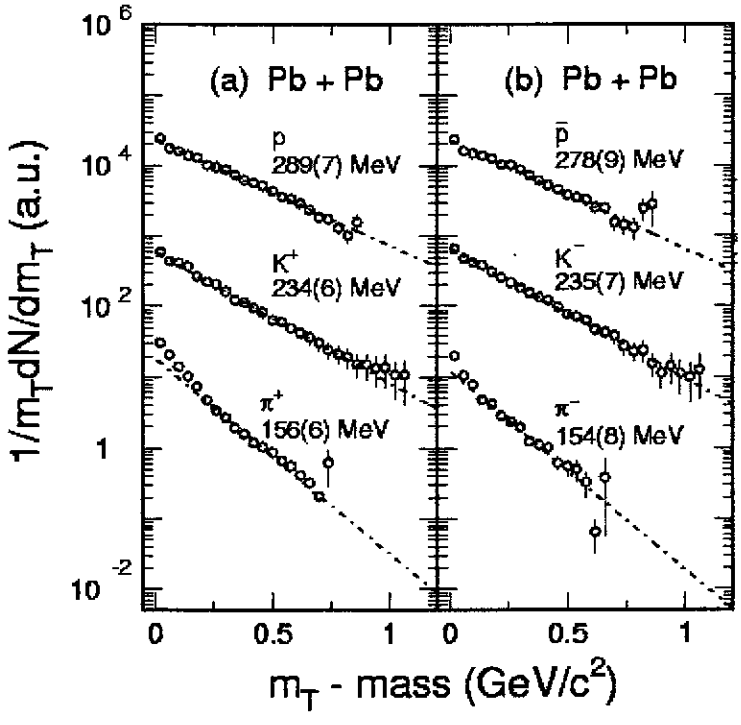

Fig. 6. Transverse mass spectra for positive (a) and negative (b) hadrons in central Pb-Pb collisions as from NA44 data. Fits by collective radial flow model is also shown: the inverse slope increases linearly with the particle mass as a result of the fast fireball expansion.

3.2.2 Electro-magnetic probes

Probes of the hot initial stage of the collision, where the most interesting phase of the nuclear matter has occurred, are based on particles with long mean free paths like direct photons that succeed to escape the plasma medium, while it is still hot, with a small probability of interacting in the outer freeze-out region since they do not undergo any strong interaction. The

(*) $\frac{1}{m_T}\frac{dn}{dm_T} \propto e^{-\frac{m_T}{T}}$

related momentum spectrum should reflect the initial temperature since direct photons are created by quarks thermalizing through collisions in the plasma.
These electromagnetic probes are therefore acting as a "thermometer" that would keep the memory of the temperature in which the thermal emission was created and hence, can serve as a diagnostic measure of the state of the system before it cooled and hadronized.
Unfortunately the shape of photon spectra is given by the laws of blackbody radiation and therefore does not provide any contents of the dynamics of the emitting source. Furthermore, there are also many other processes like the decay of π^0 and η mesons, which can produce photons, resulting in a huge amount of background.
Because of the relevant production rates of photons from hadronic reactions in the hadron gas, SPS was not able to provide unambiguous evidence of substantial thermal emission from the hot initial reaction volume, however this observable will become clearer at LHC and RHIC as both the QGP's temperature and lifetime will increase.

3.2.3 Strangeness enhancement

In usual hadronic collisions, strange particles are always produced in association resulting in a zero net strangeness, since the related quantum number is conserved in the strong interactions. The lightest strange particles are the K-meson with a mass of about 500 MeV/c^2 and the Λ-baryon (m_Λ=1115 MeV/c^2).
In chemical equilibrium, the abundance of particle species (hadrons/quarks) is governed by the Boltzmann factor, the temperature, the respective masses and the chemical potential μ[(*)]. Consequently at low temperature, production of strange quarks is suppressed because of their large effective mass (about 500 MeV/c^2).
On the contrary, in dense nuclear matter, an enhancement of strange quark production is expected in comparison to the production observed in hadronic collisions for the following two main reasons:

- once chiral restoration takes place, the strange quark mass value decreases to about 150 MeV/c^2, thus favouring the strangeness production since the temperature of the plasma will be significantly higher than the strange quark current mass;

(*) $\rho(h)/\rho(q) = (m_h/T)^{3/2} e^{-(m_h-\mu_q)/T}$

- the chemical potential for u and d quarks, which correspond to the Fermi level at zero temperature, may have a value comparable to the lighter strange quark mass. Hence, again strange quarks pairs, produced in the hot stage of the reaction, are favoured in the baryon rich environment of an ion collision since the Pauli exclusion principle pushes the creation of u anti-u and d anti-d pairs, via gluon-gluon fusion, to higher energy.

During the plasma expansion, most of the abundantly produced strange quarks and anti-quarks will not be able to encounter and annihilate into lighter quarks because they are diluted in a non-strange medium when the temperature drops. Each member of the pair, remaining frozen out of equilibrium, interacts with quarks of different flavour and eventually appears as a strange hadron in the final state.

Other mechanism than QGP could enhance the production of strange particles in the large bulk of particles created in nuclear collision. For example, some of the non-strange particles can yield new strange particles through rescattering off nucleons.

Nevertheless a particularly sensitive signature of strangeness enhancement from QGP is an excess of anti hyperons since their production energy threshold is large and because their thermal production depends on a high power of the strangeness density, whereas the non-equilibrium production in the hadron-gas phase is suppressed owing to the large mass.

In general, the ratio of strange to non strange particles and anti-strange to strange particles is expected to proceed much faster in QGP phase than by rescattering in a hadron gas as a result of the equilibration of strange and light quark flavors.

SPS data showed that the total strangeness content of the final hadronic phase is consistent with the input into hadronization expected from a flavour coalescence mechanism typical of a non-QCD perturbative quark-hadron transition (Fig.7) [10].

A further fingerprint [11] of the hadronization process has been found by plotting the overall set of particle over its relative antiparticle ratios for various species from pions to Ω hyperons (Fig.8), revealing a remarkable order in the hadronic population and temperature without the rather prominent fluctuations occurring in hadronic collisions.

Such a regularity among all the produced hadrons showing an apparent thermal equilibrium of all species can be understood as a consequence of the transition from QGP to the hadron gas phase.

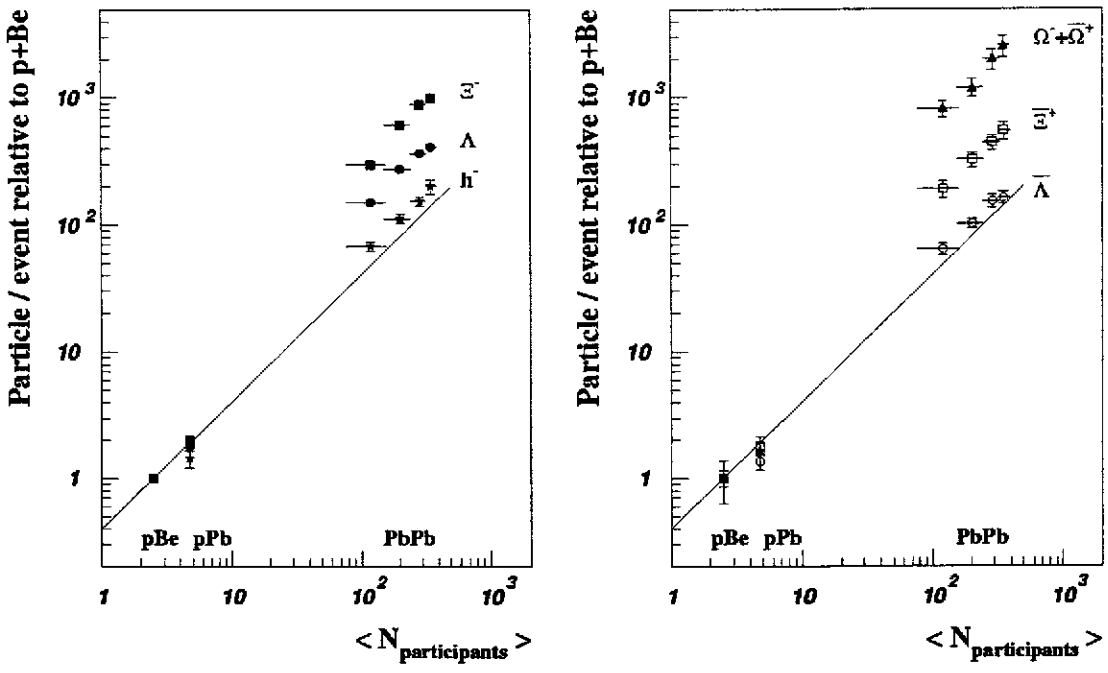

Fig.7. Strange particle production in Pb-Pb, p-Pb and p-Be as measured at the NA57 experiment at SPS.

The phase boundary appears to be located at about 170 MeV, corresponding to an energy density of about 0.6 GeV/fm^3 in agreement with the lattice QCD prediction.

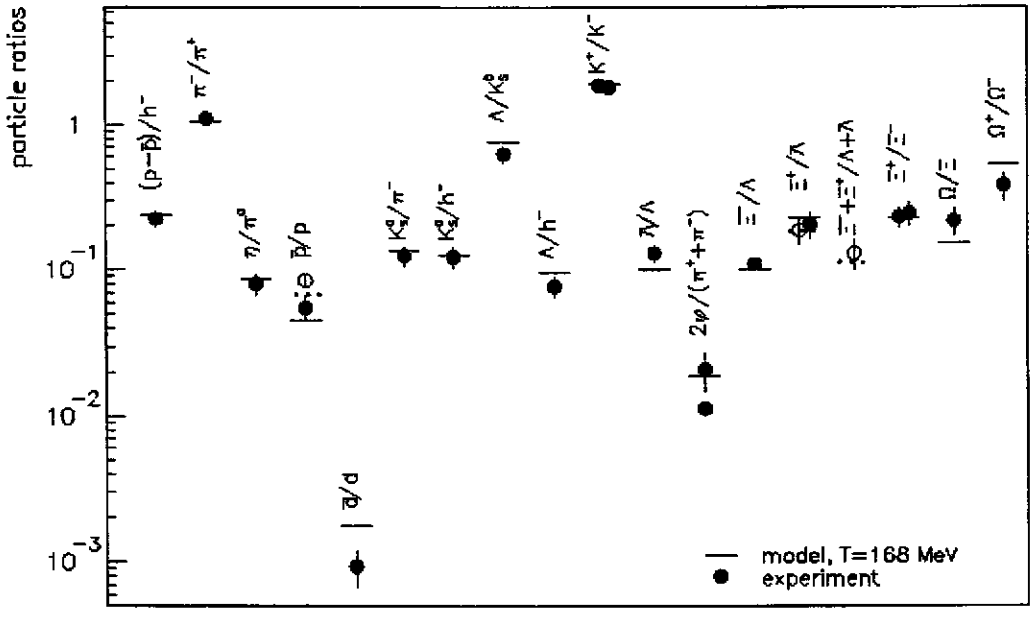

Fig.8. Compilation of particle ratios as measured at SPS (Pb-Pb central collisions). Comparison with a model of a hadron resonance gas in chemical equilibrium at T=168 MeV and baryochemical potential of 266 MeV.

3.2.4 Quarkonium state suppression

A long-lived bound state of heavy quarks (J/Ψ,χ,Ψ',ϒ)□ mainly originates from gluon-gluon fusion, generating either a c anti-c or a b anti-b pair that becomes a bound state at very early times in the collision, when the temperature is still above the charm or bottom production threshold.
In this production mechanism, it is noteworthy that the quark pair stays separate until it attains the binding distance of the relative quarkonium state. Therefore, when the reaction takes place in a medium with a high density of colour sources (quarks and gluons), a suppression of such resonances is expected since the two charmed or beauty quarks are screened from each other by the dense colour medium and cannot bind being the size of the bound state larger than the screening radius. By the time the density has decreased enough for them to bind, they meet other quarks in the dense medium thus eventually forming two charmed mesons D.
The analogy with the QED case is the Debye screening [12]. In its ground state, hydrogen atom is an insulator: the electron is bound to the proton and both experience little screening from other nearby electric charges because the atomic spacing is large. By increasing the gas pressure and therefore the density, the attractive Coulomb field between the proton and the electron is screened by the presence of other protons and electrons in the dense system. Consequently the Debye radius decreases and the electron becomes quasi-free. As soon as the Debye radius becomes comparable with the electron orbital radius, the electron will be no more able to recognize its own proton and the hydrogen atom will eventually transform into a metallic conducting object (Mott transition).
Based on similar arguments, Matsui and Satz [13], predicted that if the temperature of formation of the QGP is greater than a critical deconfinement temperature T_c, there should be a distance λ_D such that, for distances greater than λ_D the strong (colour) forces that bind the c and anti-c or the b and anti-b pair together become screened and therefore no bound state will be formed. At large transverse momenta, the charmed quark-antiquark pair, which eventually bind into a J/Ψ, have a good chance of escaping the plasma and bind outside. The suppression effect should therefore decrease at large p_T.
Quite in line with this observation the predicted pattern of charmonium suppression, due to a transient medium made up of constituents, was measured at SPS by the experiment NA50 (Fig.9) using a muon spectrometer [14].

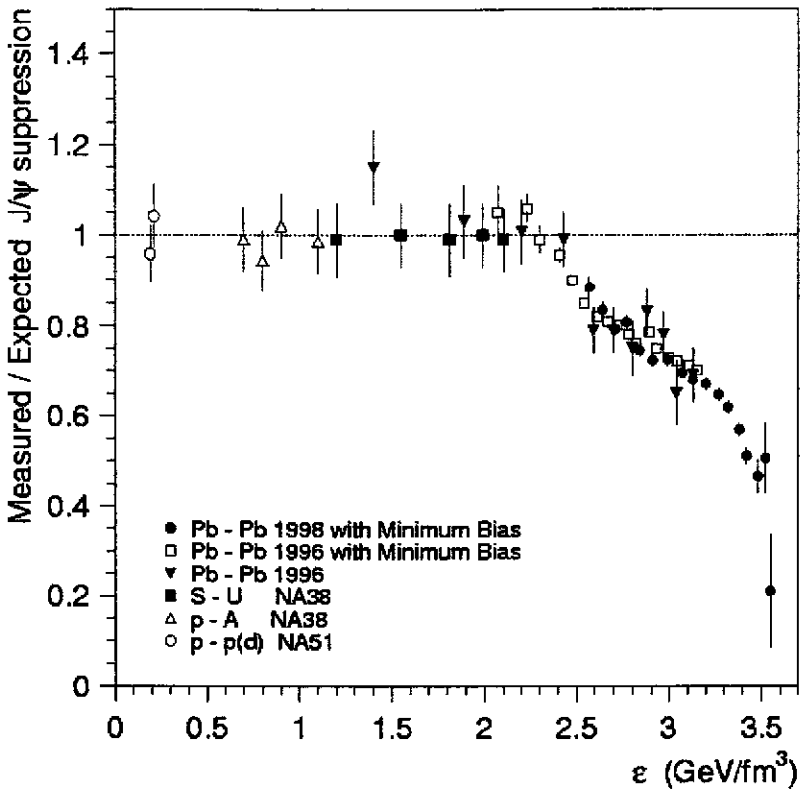

Fig.9. J/Ψ yield, normalized to Drell-Yan pair production, as a function of initial energy density.

In Fig.10 it is shown how bound states with larger size (or equivalently less tight) first disappear, ones with smaller size disappear at higher T. The Υ ground state melts at a temperature around 2 times the transition temperature. Such a high temperature will be likely reached at LHC.

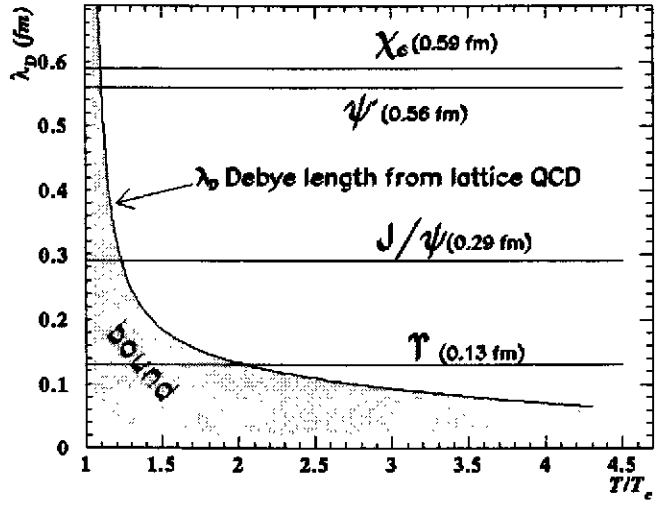

Fig.10. Debye length as a function of the ratio between the melting temperature and the transition temperature. Small size quarkonia break up at lower temperatures.

3.2.5 Low mass vector mesons

The study of vector mesons in their leptonic decay modes are difficult because of the presence of lepton pairs, produced via electromagnetic interaction of quarks and antiquarks (Drell-Yan pairs), totally independent of whether the system attains a thermalized QGP that goes through a phase transition to hadron gas.

In the 1-1.5 GeV/c^2 invariant mass region, Drell-Yan background is negligible, hence light mesons (ρ, ω and $\Phi^{(*)}$), decaying in lepton pairs with lifetimes of the order of the expansion time scale, could represent an effective probe of QGP formation. Their properties such as mass, width, and branching ratios are expected to be sensitive to strong in-medium effects and to changes in the quark masses, if chiral symmetry were partially restored.

Drastic changes have indeed been observed in electron-positron pair mass spectra thus reflecting the in-medium meson properties [15] (Fig.11). These observations are being further pursued with benefits from improved NA45 experimental facilities.

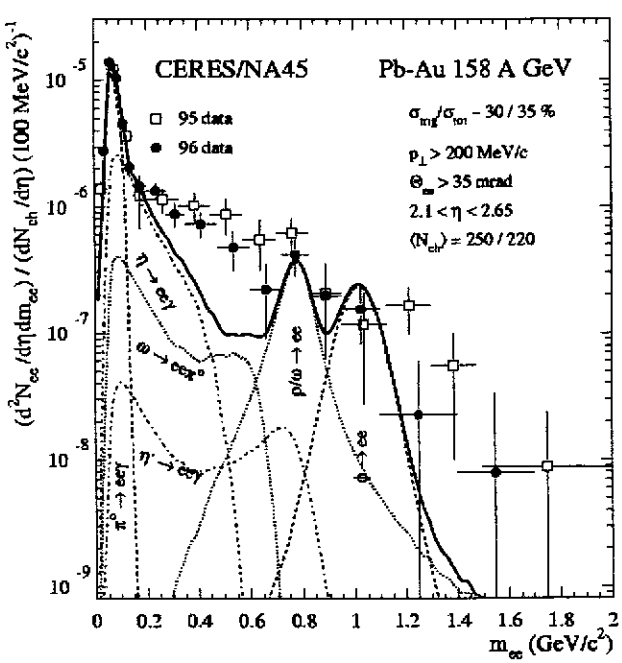

Fig.11. Background subtracted e^+e^- - pair invariant mass spectra from experiment NA45 in central Pb-Au collisions normalized to the charged particle density. Estimated contribution from meson decay is shown by the solid line.

(*) Although the same mechanism of screening holds also for s and anti-s pairs, the probability of forming a Φ(s/anti-s) remains still high owing to the large number of strange quarks created in QGP.

3.2.6 Geometrical parameters of the fireball phase

The Bose symmetry of two identical mesons imposes a correlation that depends on the size of the volume from which they originate and on the coherence that they then have thus providing helpful information on the space-time evolution of the boson-emitting source.
Meson interferometry is a generalization of the Hanbury-Brown and Twiss method in stellar interferometry.
Central Pb+Pb collisions at SPS have provided an analysis of two pion Bose-Einstein correlation data and hadronic transverse mass spectra, in terms of collective space-time parameters characterizing the "explosive" expansion dynamics of the initial dense interaction volume [16]. The overall time from formation of the "fireball" to decoupling resulted to be about 10 fm/c, long in comparison to a typical partonic relaxation time scale, of about 2 fm/c. The expanding system seems developing a strong collective velocity fields, with transverse velocity equivalent to almost 60% of the light speed, while cooling down to about 120 MeV at freezeout. These findings agree with a picture of an initial partonic cascade ending in a hadronization phase from which hadrons expand in a "blast wave" mode until decoupling.

4. RHIC and LHC

As shown in the previous paragraphs, the series of pioneering experiments at CERN-SPS in the 1990s provided an impressive evidence of the formation of a short-lived state of matter whose characteristics are very similar to the ones predicted by the lattice-QCD simulations.
However, an energy density significantly larger than that achievable by means of the 160 GeV/nucleon beam of lead nuclei at SPS, is necessary for obtaining a rather higher initial temperature resulting in a stretched hadronization time that will enable scientists to make direct observations of the plasma and to carry out a more quantitative characterization of the phase transition evolution.
A big step forward in the QGP research requires collision energy well above 100 GeV per nucleon in the centre-of-mass frame, condition that can be obtained only by using a heavy-ion collider, this being the most effective way to provide large energy to the nuclear interactions, since in fixed target collisions part of the incident energy is lost for the movement of the system as a whole.
The deployment of the two novel facilities RHIC at BNL and LHC at CERN operated with heavy nuclei, by making available a centre-of-mass energy in

the nucleon-nucleon system increased with respect to SPS by over 10 and 300 times respectively, will allow to reach initial values of energy and temperature substantially higher than the critical ones (Fig.12).

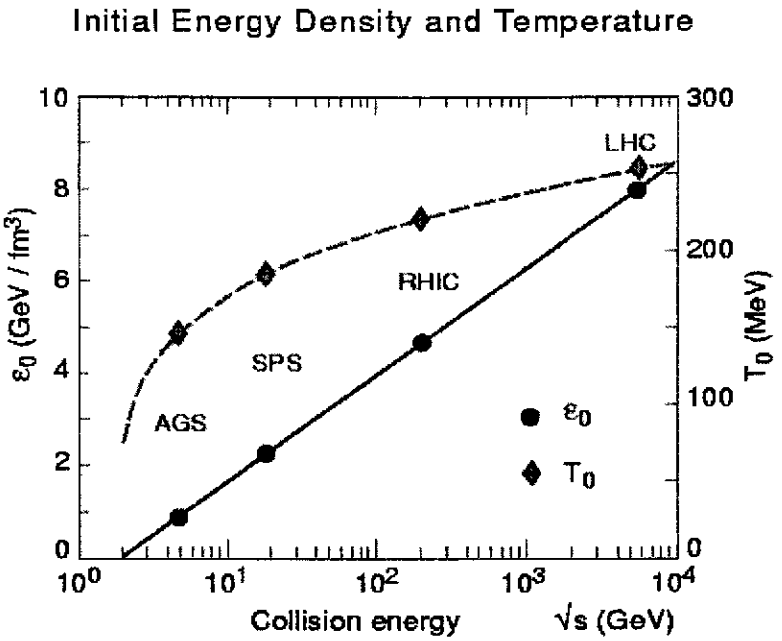

Fig.12. Initial energy density and temperature as expected at RHIC and LHC. Estimations made at BNL-AGS and CERN-SPS are also shown.

The other parameters relevant to the formation of QGP will also be favourable (Table 1): the size and lifetime of the system will improve by a large factor compared to Pb-Pb collisions at SPS thus allowing to probe QGP in its asymptotically Stefan-Boltzmann free "ideal gas" form. In particular, the lifetime is expected to be much longer than the relaxation times (which decrease in a denser system) thus allowing the system to reach and maintain thermal equilibrium throughout the expansion.

RHIC and LHC will make possible to carry out a large number of measurements, including much-improved determinations of leptonic and hadronic signals, and precise studies of even heavier quarkonium bound states like the Υ, Υ', Υ'' especially at LHC where the initial temperature will likely be larger than the melting point of this resonance family (Sect. 3.2.4). At the collider energies, high pt particle production is dominated by scattering and fragmentation of gluons that slow down faster (about 250 MeV/ fm), in the hot interaction region, owing to a colour charge larger than that of quarks.

Central collisions	SPS	RHIC	LHC
$S^{1/2}_{NN}$(GeV)	17	200	5500
dN_{ch}/dy	500	600-700	3000-8000
$V_f(fm^3)$	10^3	$7\ 10^3$	$2\ 10^4$
ε(GeV/fm^3) t_0=1fm/c	2	5	8-10
τ_{QGP}(fm/c)	<1	2-4	4-10

Table 1. Global features of central ultra-relativistic nuclear collisions as anticipated at RHIC and LHC. SPS values are also shown for comparison. ($s^{1/2}_{NN}$=centre-of-mass energy in the nucleon-nucleon system; dN_{ch}/dy=charged multiplicity per unit of rapidity; V_f=fireball volume; ε=energy density; τ_{QGP}=QGP lifetime).

Quark matter properties could be therefore investigated by looking for medium-induced modifications to the propagation of nucleon quarks and gluons that will lose part of his energy before fragmenting into a jet by interacting with the QGP's high coloured field resulting in a softening of transverse momentum particle spectra (jet quenching). As a by-product, the coplanarity of the two jets from the quarks or gluon scattering will also be destroyed entailing an azimuthal asymmetry.
The energy loss mechanism will eventually depend sensitively on the Debye screening scale of the medium and will also reduce the background from high p_t π^0's, making easier the observation of thermal radiation from QGP.
The survey of the jet quenching mechanism, not exploitable at SPS, will be an essential objective of heavy-ion detectors at the novel facilities being a firm ground for testing experimentally well-established theoretical models, since quark and gluon scattering cross sections at large transferred momentum can be calculated in perturbative QCD.
Finally, it is worthwhile noticing that the large number of particles per event produced at the colliders will allow the study of non-statistical fluctuations in a number of observables on an event-by-event basis. Anomalous

fluctuations are in fact associated with critical phenomena in the vicinity of a phase transition [17].
The main features and goals of the novel experiments are schematically outlined in Table 2.

Experiment	Facility	Features	Goals
STAR	RHIC	Very accurate tracking with a large acceptance TPC and silicon vertex trackers in a solenoidal magnetic field, particle identification capability	Global observables, event-by-event physics, high p_t physics and jet quenching
PHENIX	RHIC	Two high resolution muon arms, calorimetry, RICH, axial magnetic field	Comprehensive measurement of electromagnetic probes
PHOBOS	RHIC	Silicon strip trackers and Silicon multiplicity counters, very large event rate capability, particle identification at very low p_t	Unbiased detection of rare and unusual events
BRAHMS	RHIC	Two-arm spectrometer in fixed target configuration, high quality particle identification capability by employing TOF and Cherenkov detectors	Detailed characterization of a sub-set of particles over a broad range of rapidity and p_t
ALICE	LHC	Hadron and lepton spectrometer based on large volume TPC, silicon trackers, TOF, RICH and TRD particle identification systems in solenoidal magnetic field and a single arm muon spectrometer	Specific probes (direct photons, strangeness, low mass vector mesons, jet quenching, colour confinement) and global observables

Table 2. Main characteristics of the detector layouts ar RHIC and LHC.

5. Characteristics of collider experiment detectors

The experimental techniques employed in the heavy ion (HI) experiments are similar to those used in other High Energy Physics experiments, although the huge particle multiplicities, the lower transverse momentum range (entailing a careful control of the material for reducing the amount of multiple scattering) and the large background originated by various physics processes characterizing the collisions of ultra-relativistic heavy nuclei, make extremely difficult the design of experiments for searching the QGP. Among the above mentioned experimental issues, the very high multiplicity

of final state particles in central ultrarelativistic nucleus-nucleus collisions presents the most serious challenge for the detector systems because the total hit density could rise to such a level as to spoil detector performances.
Although the multiplicity, dn/dy_{cm}, depends on the center-of-mass energy, E_{cm}, quite weakly ($\mathbf{dn/dy_{cm} \propto \ln E_{cm}}$), it scales as the mass A of the nuclei thus reaching relevant value owing to the large mass of nuclei colliding head-on. For instance, at RHIC (Au+Au) the number of produced particles could be as high as 200 times those produced in pp interactions at the same centre-of-mass energy. Moreover, the background coming from particle decays, photon production and Drell-Yan processes scale as the square of the primary particle multiplicity and therefore the signal recognition will be affected more than in pp collisions of equal energy.
A great merit of the past experimental activity at SPS was to establish new technological directions for operating successfully in the very dense radiation environment.
In fact, although the total multiplicity was lower than that anticipated at RHIC and LHC, particle density is comparably high due to the focusing effect of the Lorentz boost in the fixed target experiments. A remarkably rapid advances in tracking detector allowed to exploit a significant physics programme by replacing the "old fashion" streamer chamber technique (Fig. 13b) with more challenging devices (Fig.13a-c).
As already stressed in the previous Sections, the identification of appropriate signatures is mandatory for surveying QGP formation and studying its properties. Therefore HI experiments are being designed in two basic configurations:

- multipurpose systems that simultaneously measure and correlate, with high accuracy, several of the most abundant observables;
- dedicated experiments that detect rare signatures with high statistics.

Both configurations must also be optimised for acquiring proton-proton and proton-nucleus events needed for searching qualitative and quantitative differences in the comparison with nucleus-nucleus events.
In the following, only the representative layout of a multipurpose HI experiment will be discussed, however some of the sub-detectors described are also employed in dedicated experiments as will be pointed out in the Sect. 6 devoted to the experiments at BNL.
A multipurpose apparatus is basically a spectrometer: a tracking system coupled to a magnetic field and a particle identification system. It covers a

large solid angle(*) in order to measure several observables in a wide rapidity interval centred at mid-rapidity where the highest energy density is expected.

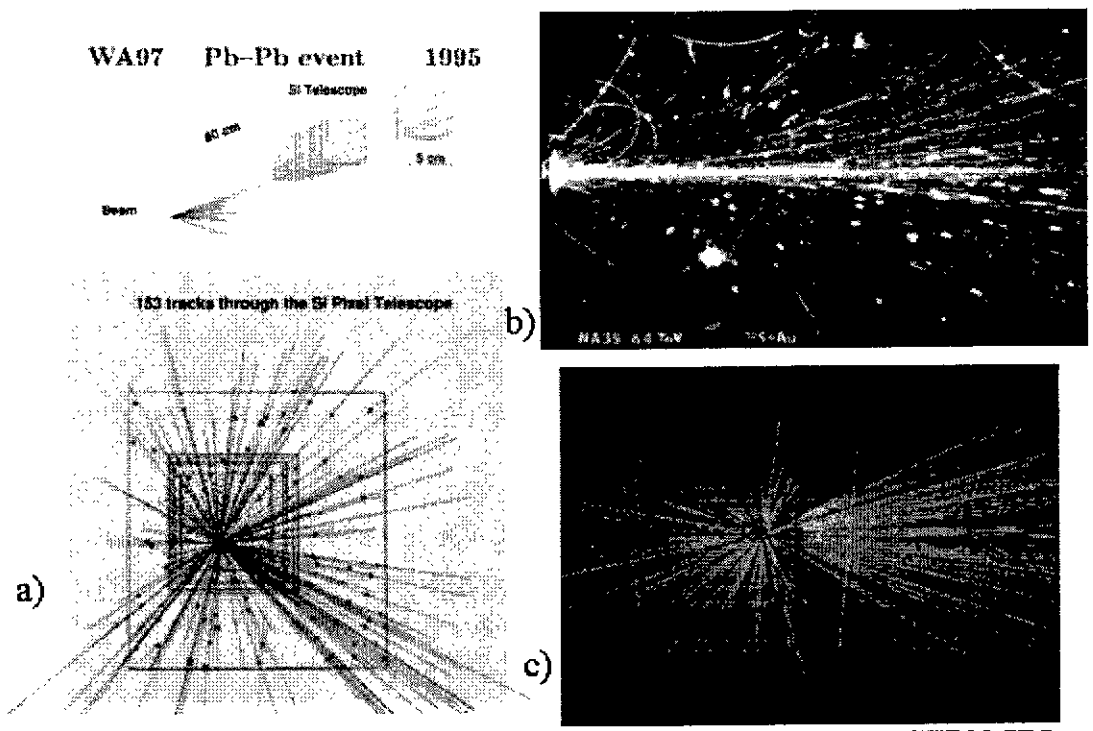

Fig.13. Examples of high multiplicity events reconstructed at CERN-SPS with silicon pixel detectors at NA57 [18] (a), streamer chamber at NA35 [19] (b) and a time projection chamber at NA49 [20] (c).

The central part has a cylindrical symmetry around the beam axis, and is embedded in a magnetic field provided by a large magnet.
Starting from the interaction point, it consists of:

- a central vertex detector designed to track charged particles emerging from the main interaction vertex and to identify decay products of short-lived secondary particles having strange and charm quark content;
- a large volume gaseous device envisaged to determine the charged particle trajectories curving in the magnetic field, allowing particle momentum and charge to be measured;
- one or more particle identification systems;
- an electromagnetic calorimeter;

(*)Coverage in rapidity of at least 2 units and 2π in azimuth is mandatory for efficiently detecting the decay products of small transverse momentum particles ($p_T<m$).

- a system for the muon detection. Muons lose a tiny fraction of their energy in traversing a dense material and therefore are identified via their high "penetrating" power. A series of absorbers will stop all incident particles but muons whose trajectories can be measured by a tracking telescope.

Some detector sub-systems will be overviewed in the following, in view of their peculiar application to HI experiments.

5.1 The tracking detectors

The working principle of a tracking device is the detection of the ionisation trail created by the charged particles traversing a medium.
Looking at the experimental probes and signatures, one realizes that tracking plays a fundamental role in HI experiments: particle identification requires the measurement of the particle momentum, strange particle recognition requires the reconstruction of the decay pattern and lepton pair measurements involve also tracking for the invariant mass reconstruction. Unambiguous space point measurements and a large number of pixels in the tracking volume (high granularity) are mandatory in the anticipated high multiplicity environment.
The reconstruction of both the primary and secondary vertices of strange and charm particles, whose proper decay lengths are typically of the order of a few centimetres and 100 μm respectively, is performed by means of a vertex detector, consisting of many concentric layers of silicon devices surrounding the collider beam pipe.
Although silicon detectors operate as ionization detectors they have the advantage to be much thinner than gaseous detectors since only 3.6 eV of energy loss is sufficient to produce an electron-hole pair; the typical thickness of few hundreds μm allows yielding a signal of some 10^4 charges per minimum-ionizing particle.
Contrarily to the gaseous tracking detector, the space resolution reachable by a silicon tracker is not limited by diffusive spreading of the ionisation cloud. Position measurements as precise as 10 μm have been achieved with silicon pixel and drift detectors (Fig.14). Both devices give two-dimensional space information in contrast to silicon strip detectors (SSD) that have a one-dimensional structure. The latter are therefore employed in the outer layers of the vertex detector barrel.
The design of the vertex detector is very challenging because of the high multiplicity and complexity of the collision's topology.
The high density of channels that characterizes these devices requires the development of highly integrated low noise read-out electronics, whilst the

large number of readout channels illustrates the necessity for cost effective chips. Moreover, the necessity of limiting the dead area regions makes the design of the access for servicing much more challenging than in the applications to fixed target experiments.

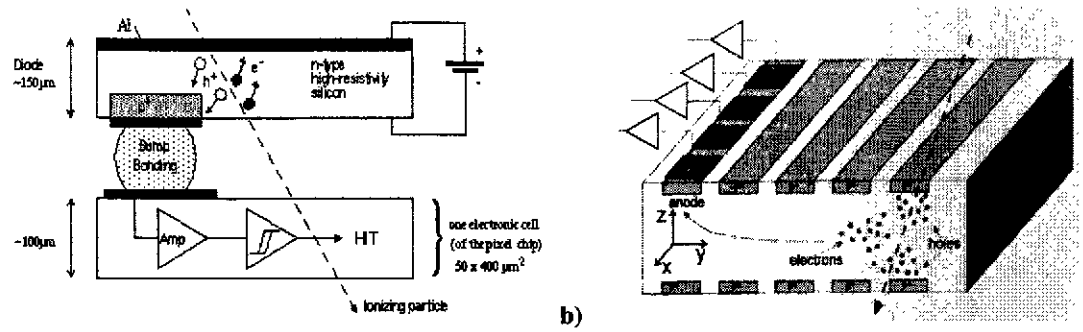

Fig.14. (a) Silicon pixel detector: the detection volume is bump-bonded to the electronic readout channel; (b) Silicon drift detector: a linearly rising potential is applied to the diode junction strips located on both sides of the silicon active volume. The resulting electric field allows to drift the electrons, created by the track ionisation, toward a segmented anode row (x-y coordinates). Drift time provides the third coordinate.

Tracking in a larger volume, at a certain distance from the interaction vertex, must be necessarily performed with gaseous detectors because of the cost effectiveness of such devices compared to that of silicon detectors.
In a collider experiment, the requirement of a maximum solid-angle coverage is fulfilled by a cylindrical time projection chamber (TPC) being a low mass device with unambiguous three-dimensional localization of tracks in a high purity gas volume embedded in a uniform electric and magnetic fields. Conventional multiwire proportional chambers (MWPC) will not be suited for this task because of their planar structure. Moreover ambiguity of hits on the wires would be too high in view of the large anticipated particle density.
The TPC's field cage is divided into two halves by a planar central electrode represented by a thin membrane and by two end cap MWPCs (Fig.15).
The primary electrons produced by ionizing particles slowly drift toward the MWPC's amplifying region where a gating grid allows their passage when triggered. If the gate is opened, avalanches are created and recorded as charge induced signal on cathode pads. Signals are inspected together with the arrival time on the wires (drift time) thus providing unambiguous three dimensional spatial measurements of the primary ionization: time measurement yields the z-coordinate along the beam direction and the wire and pad signals the x and y coordinates. The charge recorded on adjacent

pads enables an accurate determination of the position by means of the evaluation of the centre of gravity.
The large number of tracks requires the use of low gain gas mixtures and a more efficient electron gating and ion trapping for reducing the space charge effects.

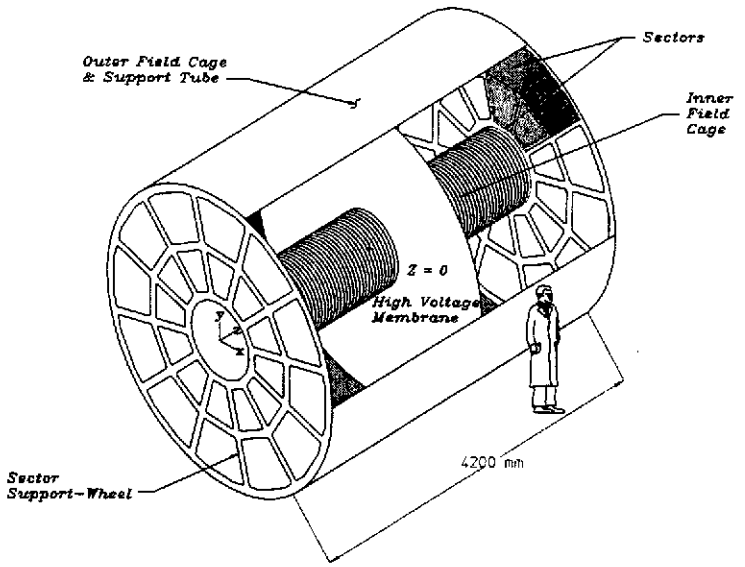

Fig. 15. Artist view of the STAR TPC. Electrons drift from the central membrane, set at a negative high voltage, toward the end-cap wheels equipped with the readout proportional chambers.

In view of the large number of electronic channels, the flux of information in a TPC is huge. Due to the fact that some channels are empty, the immediate data reduction is mandatory in order to avoid big traffic jams on the data acquisition.
Information on the track points obtained from the vertex detector combined with that provided by the TPC allows to reconstruct the entire particle trajectory. Charge sign and momentum of the particle will be eventually derived from the curvature of the trajectory in the magnetic field(*).
The random sequence of Coulomb interactions (multiple scattering) experienced by the charged particle in traversing the detector media is the main source of uncertainty in the momentum measurement.

(*) The radius of curvature, R, is given by: R (m) = 3.3 p_t(GeV/c)/B(T).

Therefore the detector structural material must be carefully selected for achieving a momentum resolution that, in the case of HI experiments, is determined:

- at low p_t, by the meson interferometry of big size sources. The uncertainty relationship ($\Delta x \cdot \Delta p \leq 197$ MeV·fm) provides the accuracy needed in the momentum measurements of the two bosons. For a source size bigger than 1 fm, the momenta of the two bosons must be measured with an accuracy better than about 200 MeV/c;
- at intermediate value of p_t, it must be of the same order of the natural width of ϕ mesons for studying the mass and width of this resonance in the dense medium;
- at large momenta, resolution should be such to allow the study of the spectra of the leading particles in the jets.

5.2 Particle identification

At RHIC and LHC energies, more than 97% of the particles are produced with a p_t<2GeV/c, the bulk of the remaining 3% will be in the range 2-5 GeV/c although a not negligible fraction (~0.02%) will have a $p_t > 5$ GeV/c. Therefore more than one method is needed for an efficient particle identification (PID). However PID can be performed on a statistical basis for the determination of the temperature as deduced from the transverse momentum spectra and of the mean transverse mass for different particle species. On the contrary, particle interferometry measurements and evaluation of ratios between particle species require a more demanding particle identification ($\geq 3\sigma$ separation) on a track-by-track basis.
Hadrons are identified by measuring their mass if the momentum p and the particle velocity are known(*).
Low momentum hadron identification can be achieved via measurements of energy loss in the silicon layers and in the TPC field cage gas, while above the $1/\beta^2$ region, identification is performed by employing time-of-flight (TOF) detectors (Fig. 16).
At the collider experiments, the TOF technique is extremely challenging above 2 GeV/c because of the limited size of the flight path, whereas an approach based on detectors that exploit the emission of Cherenkov radiation from charged particles traversing an optical medium with a velocity higher than that of light in the same medium is more suitable for the favourable performance over cost effectiveness ratio.

(*) $m=p/\beta\gamma c$, with $\beta=v/c$ and $\gamma=(1-\beta^2)^{-1/2}$

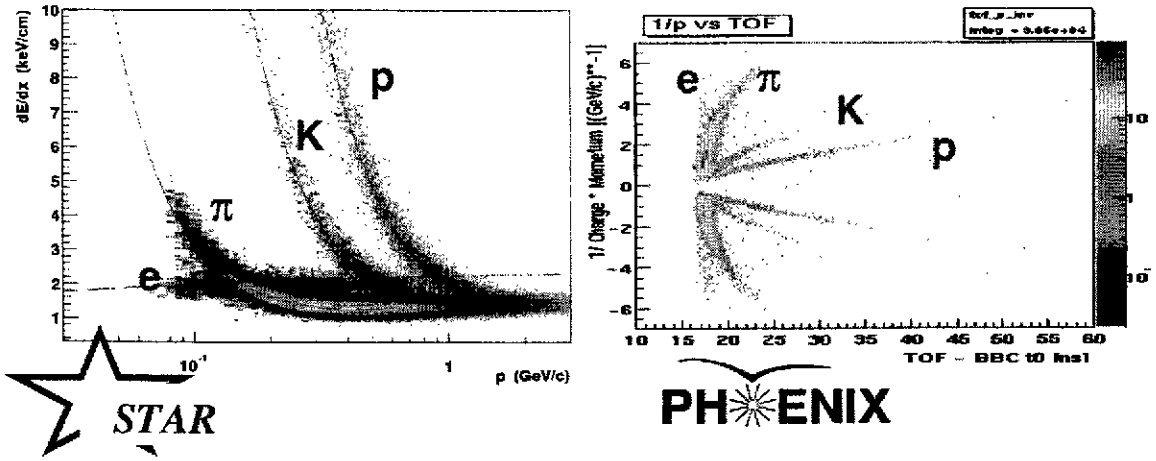

Fig. 16. Particle identification as achieved by STAR with energy loss measurements in the TPC and by PHENIX with TOF measurements.

More specifically, Ring Imaging CHerenkov (RICH) detectors, being able to determine the position of each of the Cherenkov photons converted into photoelectrons by a suitable photocathode, are used for their capability to measure the Cherenkov angle with an error of few mrad. This accuracy is sufficient to discriminate π, K and p in the relevant momentum range. Since its inception, RICH technology has continually benefited from new developments in the field of photon detectors, first using photosensitive vapours (TMAE, TEA), then exploiting CsI thin films deposited onto the cathode plane of a MWPC (Fig.17).

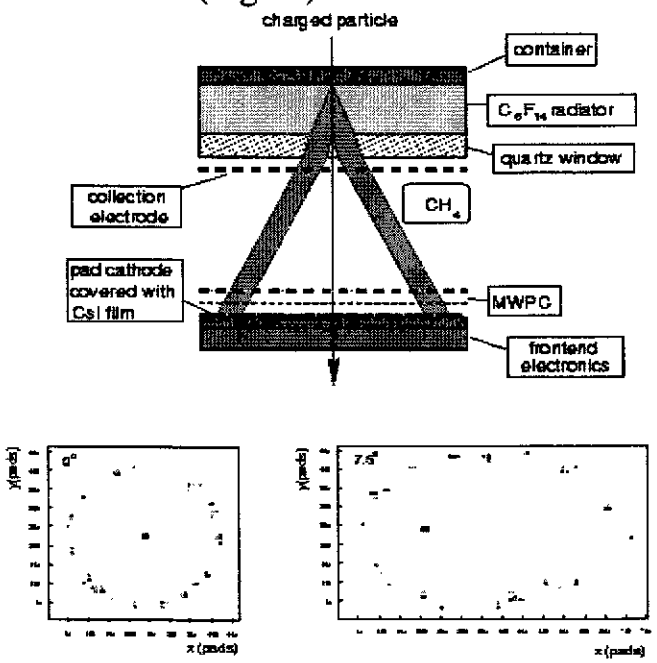

Fig.17. Working principle of the CsI RICH detector at STAR and ALICE [21]. A layer of photosensitive CsI film, evaporated on one of the MWPC's cathode, converts the Cherenkov photons into single electrons. The resulting single event images are shown, at the bottom, for 0° and 7.5° incidence angle, respectively.

Electrons are identified by employing transition radiation detectors (TRD). Transition radiation in the X-ray region occurs when a charged particle with a factor $\gamma \geq 10^3$ crosses the boundary between two media with different dielectric constants. TRDs consist of a radiator containing a discontinuous medium represented either by a stack of several hundred foils (Mylar, polyethylene or lithium) or by a foam (carbon fibers...) followed by a wire chamber filled with heavy gases (Xe or Ar) for the detection of the transition X-rays (Fig.18). The detection of the transition radiation is complicated by the presence of the particle ionization energy loss in the chamber gas. In fact on the contrary of the Cherenkov radiation, X-rays are emitted highly collimated along the particle track (emission angle ~ $1/\gamma$), thus limiting the hadron rejection capability to about 10^2.

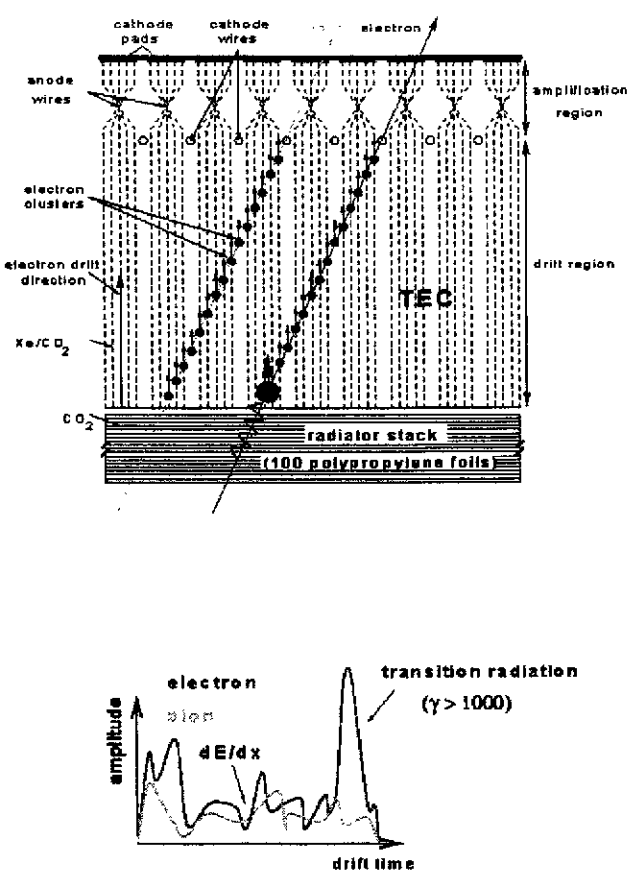

Fig.18. Working principle of the ALICE TRD [22] detector based on a time expansion chamber: the transition radiation X-rays, being converted into electrons as soon as they enter the gas region, will be detected after a longer drift time than the ionisation trail along the particle track.

5.3 Trigger detectors and beam counters

Specific beam counters are mandatory in the case of HI experiments because of the necessity to exploit the entire centre-of-mass energy available from the collider for achieving the most extreme conditions of high density and temperature in the nuclear matter.
Some beam nuclei loose part of their nucleons in interactions with the atoms of residual gas in the vacuum of the beam pipes. These nuclei do not carry the full energy and have to be identified by a detector placed upstream of the interaction region in order to separate them from the "good" beam nuclei. Such a detector must be fast and must have a high separation power for distinguishing nuclei of different size.
The interesting central collision events that must be selected and analysed for searching signals from QGP are characterized by small impact parameters. Only few percent of the collisions will be nearly central, consequently an efficient trigger counter must be designed to provide information on the collision geometry.
In head-on events, a small fraction of spectators from the colliding nuclei emerge with small transverse momenta from the collision releasing a small energy in the "zero degree calorimeter" located downstream the interaction region. An alternative way to the energy flow measurement is to look directly for the missing beam energy by counting the number of the secondary charged particles emitted in the collision(*). Such a measurement is performed by employing silicon "multiplicity detectors" which surround the interaction region.

6. RHIC

RHIC (Relativistic Heavy-Ion Collider) [23], commissioned at Brookaven National Laboratory (BNL) in 2000, is the first purpose-built facility completely dedicated for heavy-ion physics making available a variety of

---

(*) Rather than the polar angle θ, one utilizes the pseudo-rapidity η defined as:

$$\eta = -\log tg\frac{\theta}{2}$$

which is a good approximation for rapidity in the limit when the particle mass can be neglected ($p, p_T >> mc$). It can be measured without knowing the momentum of the particle.

nuclei up to Au at a centre of mass energy of 200 GeV/A and protons up to 500 GeV.
RHIC consists of two 3.8 Km long concentric vacuum sections (Blue and Yellow Rings) of super-conducting magnets in which Au beams circulate in opposite directions and cross at six interaction regions (Fig.19). It is designed for a Au-Au luminosity of about 2 10^{26} cm^{-2} s^{-1} at top energy.
It takes almost one minute to fill each Ring by injecting a total of 60 bunches, successively nuclei are accelerated to 100 GeV per nucleon and left circulating and colliding for about ten hours.
Although RHIC is capable of colliding heavy nucleus beams in six interaction regions, only four detectors are currently running, although not fully instrumented because of insufficient funding, two with a large layout (STAR and PHENIX) and two smaller ones (PHOBOS and BRAHMS).

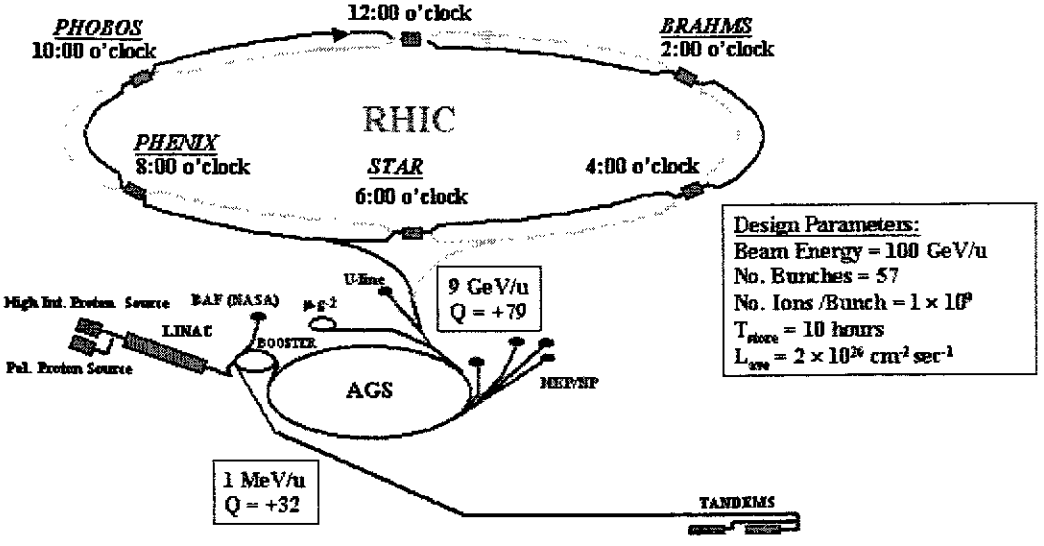

Fig.19. RHIC accelerator complex. Nuclei are accelerated from the tandems through the transfer line into the Booster and then into AGS prior to be injected into RHIC's Rings.

Each experiment exploits a variety of detection techniques and is designed to be complementary to one another in order to cover almost every proposed observable of QGP formation.

6.1 STAR

STAR (Solenoid Tracker At RHIC) is a high granularity 4π detector with emphasis on accurate tracking and precise impact point localization designed to measure mainly global features of identified hadrons and jets on a event-

by-event basis and on the study of hard scattering processes between nucleon constituents [24].
An artist view of STAR is shown in Fig.20. Moving out from the beam axis, in the large volume solenoidal magnet at 0.5 T, the first element is the silicon vertex tracker (SVT) consisting of three layers of silicon drift detectors arranged in cylindrical barrels providing a spatial resolution of 20 μm necessary for the reconstruction of hyperon and charmed particle decay vertices.
Moreover SVT improves the momentum resolution for high p_t particles, allows tracking and identification via dE/dx in the $1/\beta^2$ region for low p_t particles and the definition of the angles for tracks used in the particle interferometry measurements.

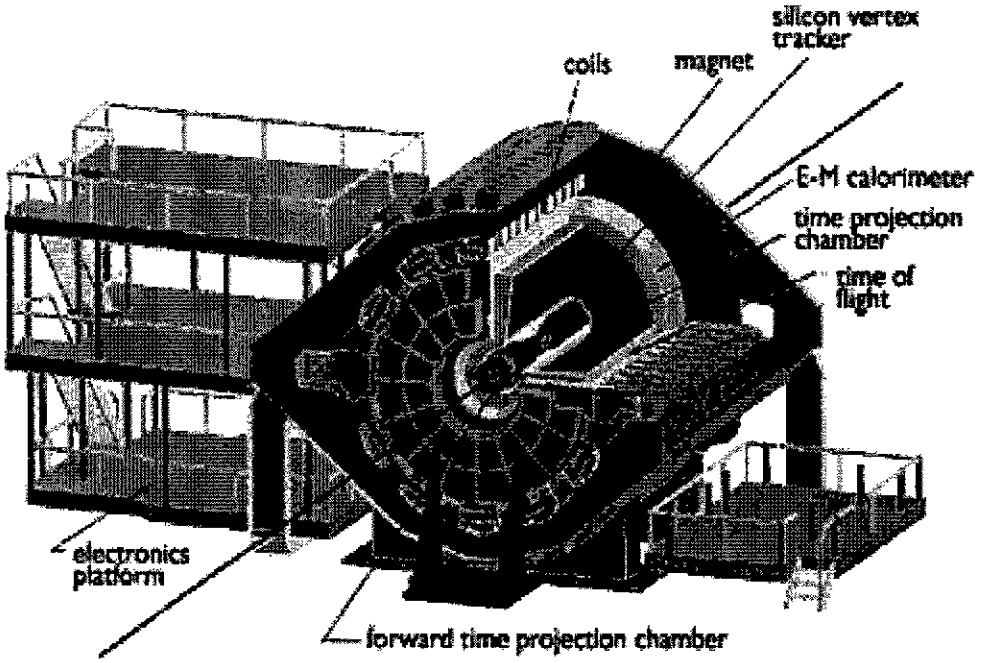

Fig. 20. Artist view of the STAR experiment at BNL.

SVT is followed by a TPC (with a diameter of 4 m and a length of 4.2 m) covering 4 units of rapidity with full azimuthal coverage.
Size and configuration of the pads of readout chambers have been optimised in order to provide the best accuracy in the energy loss measurements and the highest tracking resolution and double track separation power. On both edges of the TPC, there are 12 rows of pads arranged along radial sectors for a total number of 137000 pads. In the innermost sector, pads have the minimum size (2.85x11.5 mm^2) thus providing the best two track separation. The outermost pads are 6.2x19.6 mm^2.

Momentum resolution is given by:

$$\frac{\delta p_T}{p_T^2} \approx 0.01(GeV/c)^{-1}.$$

For particle tracks at high pseudorapidity ($|\eta|>1$), the momentum resolution worsens as the curvature R_{out} of tracks moving out from the TPC gets shorter:

$$\frac{\delta p_T}{p_T^2} \approx 0.01 \times \left(\frac{R_{TPC}}{R_{out}}\right)^2 (GeV/c)^{-1}.$$

An array of 240 scintillator slats, lying just outside of the TPC outer field cage constitutes the central trigger barrel (CTB) that provides fast charged particle multiplicity information and define the centrality of the interactions in association with measurements of beam fragments carried out by two calorimeters at small forward angles (ZDC).

The STAR data acquisition system can record about 2 central interactions per second. CTB is followed by a highly segmented TOF array to increase the pion/kaon and p/kaon separation power. The last layer of STAR is a Pb-scintillator sampling electromagnetic calorimeter (EMC) used to trigger on transverse energy and measure jets, photons and electrons. It consists of a barrel ($-2 \leq y \leq 2$, $\Delta\phi=2\pi$) and one endcap. Two additional end-cap TPCs located in the forward regions ($2.5<\eta<4$) will extends the acceptance to near beam rapidities.

In 1999, STAR complemented its particle identification at low momenta (achieved with the TPC and SVT until 0.6 and 1 GeV/c, for kaons and protons, respectively) with a patch of detector dedicated to high momentum identification, based on the Ring Imaging Cherenkov technique.

It covers the central rapidity region $\Delta\eta<0.3$ and $\Delta\phi=20^0$ and allows to extend the momentum range of particle identification to ~ 3 GeV/c for kaons and 5 GeV/c for protons (Fig. 21). Such a detector was originally built as a prototype for the ALICE experiment at the LHC.

The STAR collaboration consists of 400 participants from 33 institutions in seven countries.

6.2 PHENIX

PHENIX (Pioneering High Energy Nuclear Interaction experiment) was primarily designed to observe the leptonic and electromagnetic signals of QGP formation, i.e. electron and muon pairs and photons [25].

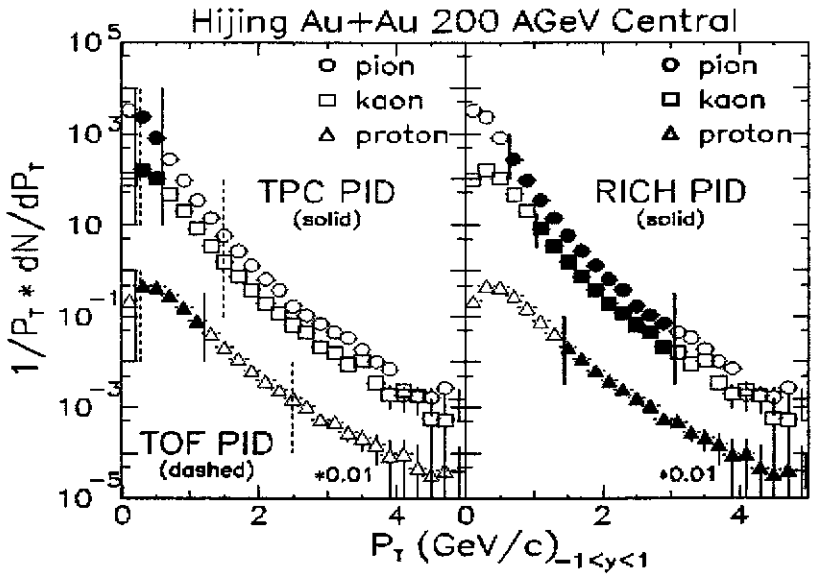

Fig.21. Invariant distribution of p_T for π, K e p, in Au-Au collisions at 200 AGeV/c as estimated by HIJING (Heavy Ion Jet INteraction Generator). Identification capability of TPC, TOF and RICH are shown. RICH extends the identification range for protons up to 5 GeV/c.

The schematic layout of the experiment is shown in Fig.22.
It comprises four spectrometers: two forward muon arms on both sides and a steel magnet providing an axial field along the beam axis, with two central left-right detectors each covering $-0.35 \leq y \leq 0.35$ and 90° in azimuthal angle. The central arms includes, from inside to outside : a silicon multiplicity vertex detector, an inner tracking system of two sets of drift chambers and a pad chamber as tracking detectors, a RICH, a time expansion chamber sandwiched between two pad chambers and em calorimeter for photon measurements.
The demanding electron/hadron separation is achieved by means of both the RICH and the calorimeter. In addition to leptons, the inclusive spectra of pions and kaons would be accessible to some extent by equipping a smaller part of one arm with high resolution TOF counters. The muon arms contain detector elements to perform charged particle tracking, momentum measurement and muon identification. The steel yoke of the central magnet is used as the primary hadron absorber. Those particles which emerge from the pole tip enter the muon arm which exploits the radial field produced by the muon magnet to perform momentum measurements. Trajectories are measured in multi-layer drift chambers arranged in three stations. Downstream of the muon magnet, muons are distinguished from pions and other shower products by means of a muon identifier, consisting of concrete

absorber walls interleaved with planes of streamer tubes. The coverage of the muon detection extends from $1.1 \leq \eta \leq 2.4$ (10°-35°).
Light vector meson characteristics (width and position of mass spectrum) will be sensitive to the medium, especially the ρ-meson with its rather low lifetime ($c\tau \approx 1.3$ fm compared to the lifetime and size of the hot fireball < 10 fm).
PHENIX is the most suited experiment for these studies although a low signal-background ratio of 1:35 is expected in view of the presence of a high combinatorial background. The huge weight of the layout (3000 tons) and the largest collaboration at RHIC (>450 researchers from 45 institutions in 10 countries) makes PHENIX bigger than STAR although much fewer particles than STAR are detected per event.

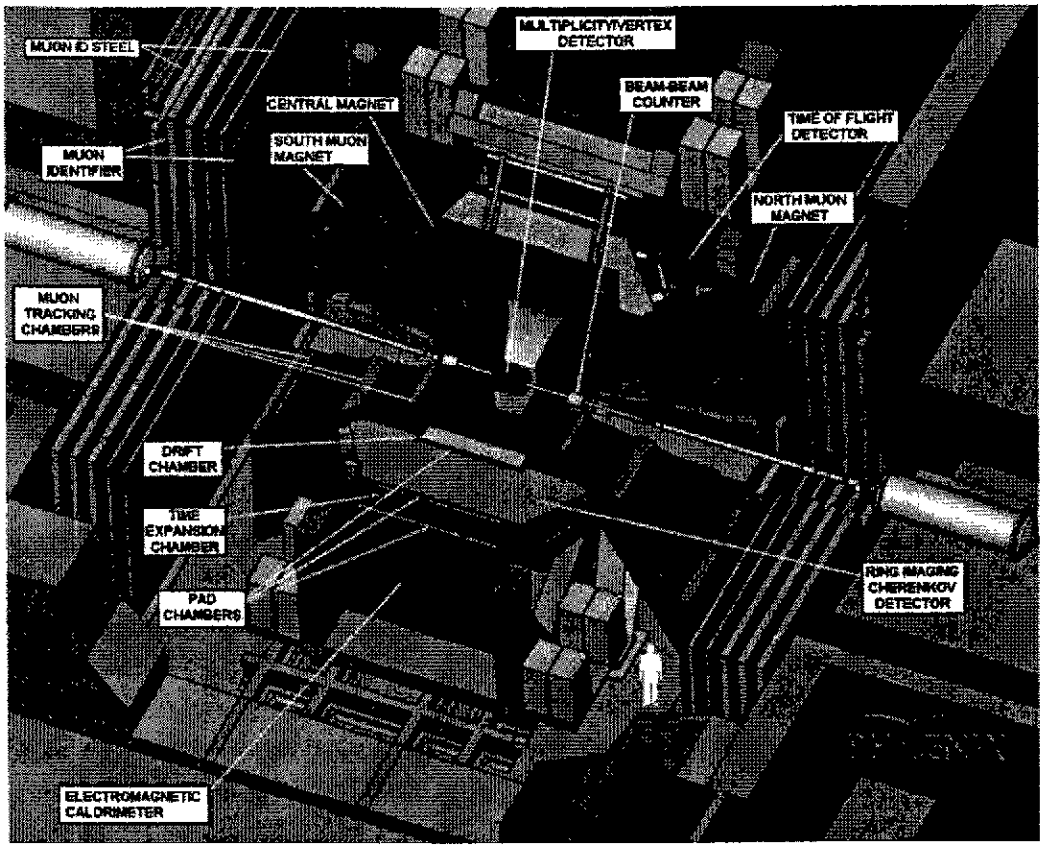

Fig. 22. The PHENIX experiment layout.

6.3 PHOBOS

PHOBOS is an experiment, based on silicon-detector technology, designed to look at RHIC collisions in an unbiased way (high rate, minimum bias data taking up to 600 Hz as expected at the nominal luminosity) [26].

Its goal is to detect rare and unusual events and to study in detail about one per cent of the produced particles, including measurement of charged hadrons, and possibly K_s^0 and lambda in the central region.
PHOBOS consists of a multiplicity detector covering almost the entire rapidity range of the produced particles ($-5.4 \leq y \leq 5.4$) with whom the events will be characterized and a two arm spectrometer at mid-rapidity located on either side of the interaction volume, as shown in Fig.23. Each arm covers about 0.4 rad in azimuth and the pseudorapidity range $0 \leq \eta \leq 2$ depending on the interaction vertex, allowing the measurement of p_t down to 40 MeV/c and PID for almost 1% of the produced particles by employing a TOF array. In such a way, a broad view of each event along with detailed information about a small subset of the fragments ejected from the plasma will be obtained. Seventy researchers from 12 institutions in three countries are working on PHOBOS.

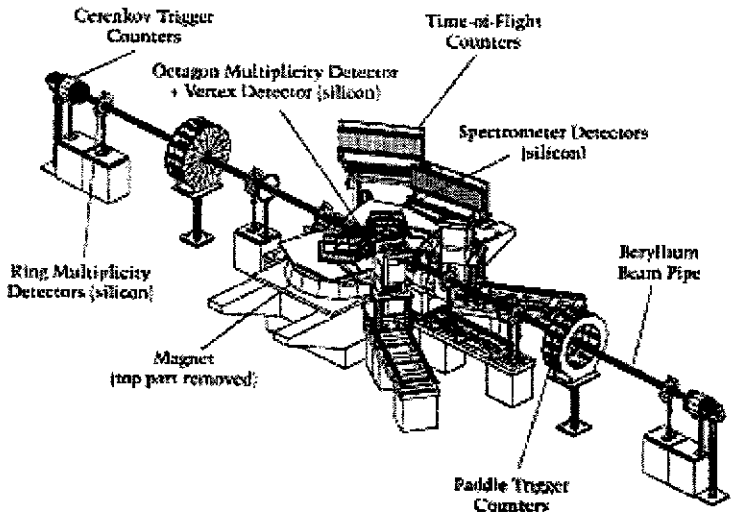

Fig. 23. The PHOBOS experiment layout.

6.4 BRAHMS

Currently, 51 participants from 14 institutions in eight countries are involved in the experiment BRAHMS (Broad Range Hadron Magnetic Spectrometer) based on a movable two-arm spectrometer capable of measuring identified charge particle spectra over a wide range of rapidity and transverse momentum from the central region to very close to the beam axis, depending on the position of its arms [27] (Fig. 24).
The midrapidity spectrometer covers the range: $0 \leq \eta \leq 1.3$ and is capable of identifying charged particles with $p<5$ GeV/c by means of a TOF wall and

segmented gas Cherenkov counters. Tracking is achieved by employing two TPCs and a magnet for momentum measurement. The forward spectrometer has a solid angle acceptance of 0.8 mstr, covering $1.3 \leq \eta \leq 4.0$. It consists of four dipole magnets, three TPCs followed by drift chambers. PID is provided by TOF hodoscopes, one threshold Cherenkov and one RICH. It will determine the K/pion ratio over a large rapidity interval and measure high transverse momentum particles.

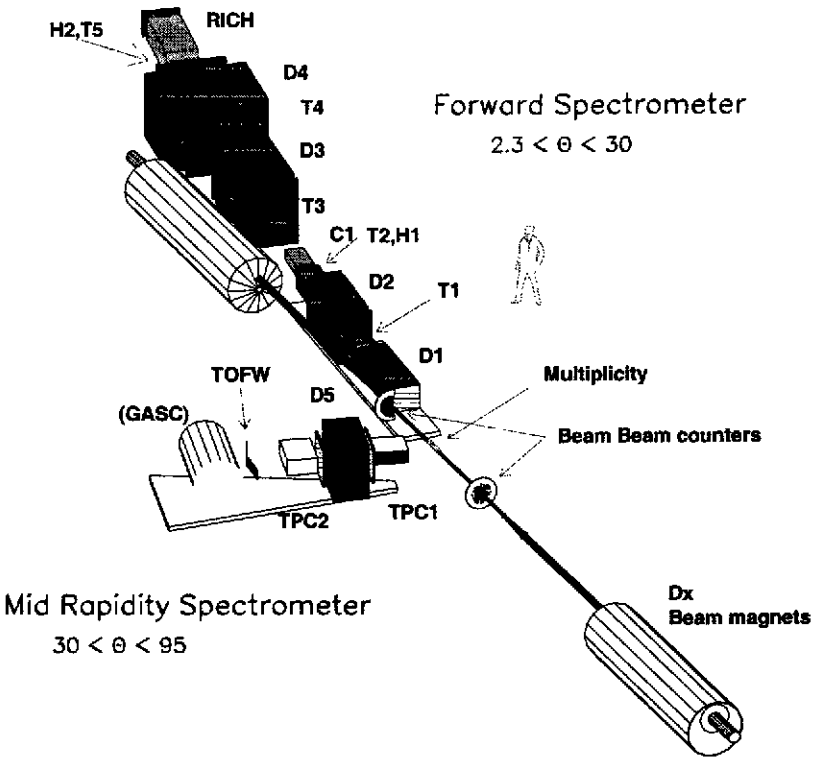

Fig. 24. The BRAHMS experiment layout.

7. LHC

LHC operated with Pb on Pb at a center-of-mass energy of 2.75 TeV/nucleon with a luminosity of 10^{27} $cm^{-2}s^{-1}$ will be the ultimate facility for searching QGP. It will also be possible to accelerate lighter nuclei (at higher luminosity) and in principle also asymmetric systems like pA interactions [28].

Since LHC operations with lead beams is likely to reach a luminosity of $2x10^{27}$ $cm^{-2}s^{-1}$, an interaction rate of about 10^4 Hz is expected, but

fortunately only a small fraction, approximately 2-3%, corresponds to the most interesting central collisions with maximum particle production.
It follows that the requirements on the detectors are much less stringent than those in LHC pp experiments, and allows to exploit slow devices like TPC and silicon drift detectors, although, as already pointed out, the high multiplicity represents in this case a very demanding task when it combines with the large rapidity range to be covered.

7.1 ALICE

ALICE (A Large Ion Collider Experiment) is the only dedicated experiment planned for the CERN LHC to investigate heavy ion collisions at center-of-mass energy of 2.75 TeV per nucleon [29]. The uneasy role of being alone at LHC for this kind of physics (apart for the CMS experiment which will have some very limited capabilities for nuclear collision studies) conditioned its design. In fact, ALICE is meant as a general-purpose experiment with a single set-up whose design has been optimized to study both hadronic and leptonic signals together with a global survey of the events.
It is designed to cover a wide range of momenta (from 60 MeV/c up to 10 GeV/c) and identified particles (from the electron to the Υ's resonances) and cope with the highest particle density anticipated for Pb-Pb collisions at the LHC (theoretical models predict up to 8000 charged particles per unit of rapidity for central Pb on Pb collisions). Interactions between lower mass nuclei and p-p will also be studied as reference data for the nucleus-nucleus collisions.
Currently, more than 900 physicists from 70 institutions in 25 countries are involved in building ALICE piecewise in an international jigsaw puzzle.
From the artist view of the lay-out, shown in Fig.25, one immediately recognizes that ALICE consists of two main components: a 2π barrel detector system at mid-rapidity (polar angles from 45° to 135°) embedded within the 0.2-0.4 T uniform solenoidal field provided by the large magnet formerly used in LEP's L3 experiment and a forward muon spectrometer (from 2° to 9° polar angles).
The following detectors, starting from the beam axis, are sheathed in the L3 magnet:
- an inner tracking system (ITS) with six cylindrical layers of highly accurate position-sensitive silicon detectors;
- a cylindrical, large volume, time projection chamber (TPC);

- two large area and highly segmented particle identification arrays for hadrons (TOF) and electrons (TRD);
- a single arm particle identification device for higher momentum hadrons (HMPID);
- a single arm outer electromagnetic calorimetric complex (PHOS) located below the central barrel region.

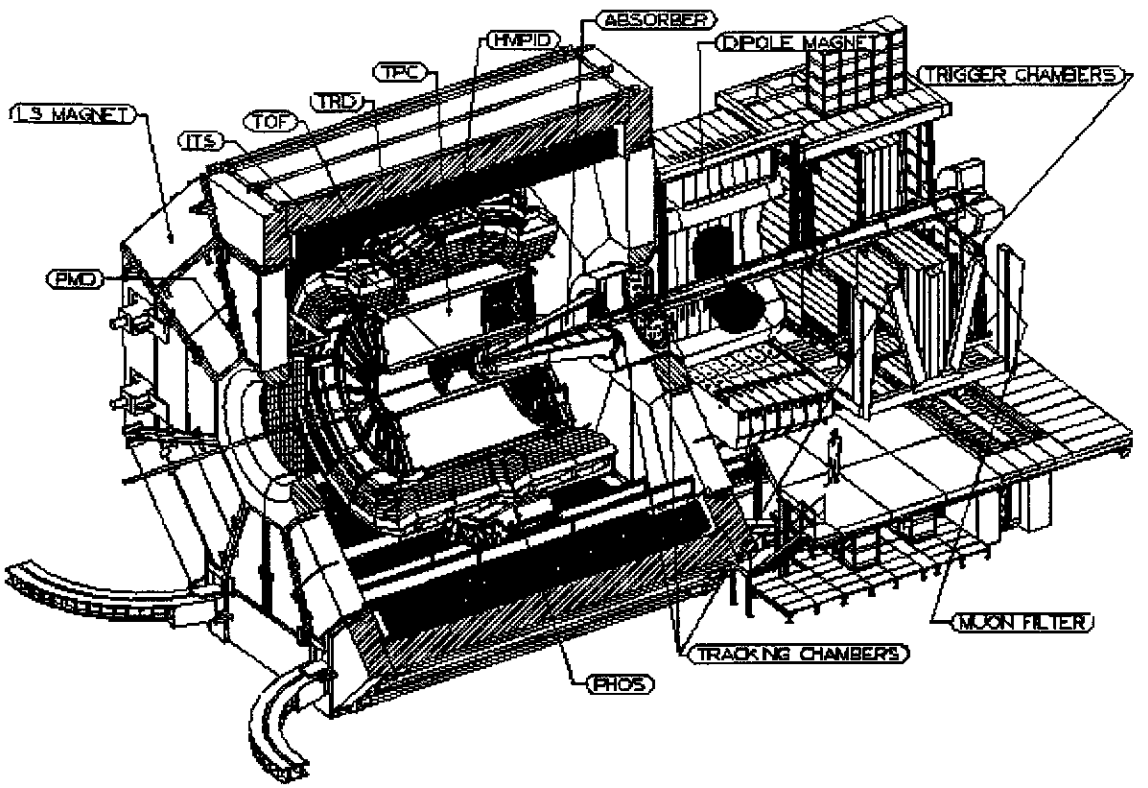

Fig. 25. The ALICE experiment layout.

Four small and very dense zero degree calorimeters, made of tungsten and lead with embedded quartz fibres read out by PMT's complete the set-up. They are located about 100 m downstream the machine tunnels on both sides of the interaction region to measure and trigger upon the impact parameter.
The innermost planes of ITS are made of truly bi-dimensional devices, pixel and drift detectors, owing the high particle density expected whereas the two outer planes are made of silicon microstrip detectors.
ITS is located as close as possible to the beam axis and has the task of tracking particles of very low momentum, identifying short-lived particles (mostly hyperons) decaying before they reach the TPC, and improving the momentum resolution of the tracked particles. Drift and strip silicon layers will be equipped with an analog readout for independent particle identification via dE/dx in the $1/\beta^2$ region.

The TPC is designed to provide tracking, momentum and dE/dx measurements for charged particles with pseudo-rapidities in the range $-1<\eta<+1$. It has an active volume defined by the two cylindrical surfaces at r= 90 cm and r= 250 cm. The inner radius is given by the maximum acceptable density of hits in the inner TPC volume whilst the outer radius is determined by the minimum track length required for achieving a dE/dx resolution better than 10%. The role of TPC is crucial for achieving good two-track resolution in order to cope with the expected high multiplicity events.
Particle identification (PID) in the full range of momentum is crucial for the physics that ALICE is designed to study, indeed TOF and HMPID systems enhance PID capability in the momentum range covered by energy loss measurements in ITS and TPC and allow to identify particles at much higher momenta than using dE/dx alone.
Namely, the TOF barrel is being optimized for the identification, on a track-by-track basis, of hadrons with a transverse momentum below 2 GeV/c, with a separation between pions and kaons better than 3 sigmas while HMPID is being designed to extend the useful range to 2.7 GeV/c (and up to 5 GeV/c for protons).
An array of multigap resistive plate chambers is the current solution for the low momentum PID system while the Ring Imaging Cherenkov (RICH) technique is the preferred option for the HMPID.
The TOF barrel covers a surface larger than 100 m^2 at a radius of about 3.5 m. Time resolutions as good as 70 ps are aimed for since a separation power greater than 3σ is required on a track-by-track basis to keep the contamination below a 10% level in the presence of a huge bulk of hadrons at low momentum. The TOF groups are working on scaling up an innovative device consisting in a stack of resistive plates, spaced one from the other with equal sized spacers creating a series of gas gaps, each 250 μm thin. Electrodes are connected to the outer surfaces of the stack of resistive plates while all the internal plates are left electrically floating (Fig. 26). Time resolutions as good as 65 ps have been achieved on small size prototypes.
HMPID will consists of an array of CsI RICHs covering about 12 m^2 thus representing the largest scale application of such a technique.
The radiator is a 1.5 cm thick layer of low chromaticity C_6F_{14} (perfluorohexane) liquid with an index of refraction of n=1.2834 at λ=175 nm corresponding to β_{min}=0.78 (i.e. a threshold momentum p_{th}(GeV/c)=1.26 m, with m equal to the particle mass in GeV/c^2). The Cherenkov cone refracts out of the liquid radiator of C_6F_{14} and expands in the proximity volume of CH_4 before reaching the MWPC photon detector thus allowing a better imaging of the Cherenkov pattern (Fig. 17).

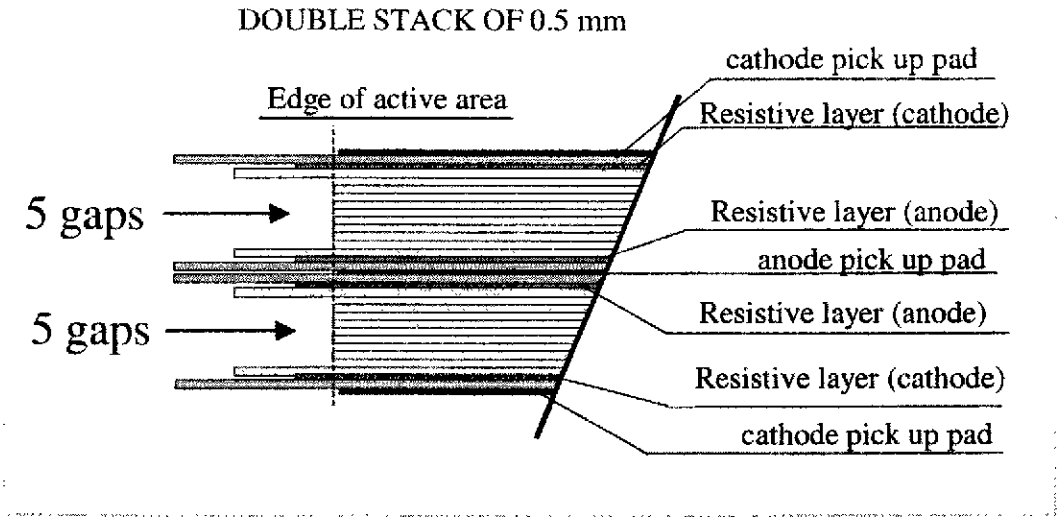

Fig. 26. Schematic of the Multigap Resistive Plate Chamber employed as TOF detector at ALICE.

Physics motivations for the single arm HMPID detector are the determination of inclusive particle ratios and transverse momentum spectra in the dense region of the mini-jets that dominate the pre-equilibrium stage of the nucleus-nucleus collisions.
Therefore, the HMPID is expected to provide useful information on jet quenching by measuring the ratio of high p_t proton/antiproton spectra and to allow extending p_t range where Bose-Einstein interferometry with kaon pairs can be studied. In fact, KK correlation will be less influenced by resonance decays after hadronic freeze-out than pionic correlations.
The TRD will identify electrons with momenta above 1 GeV/c to study quarkonia suppression and heavy quark production (charm, beauty) near mid-rapidity. It consists of six layers of xenon-filled time expansion chambers with a radiator stack of carbon fibers.
A pion rejection capability of less than 1% at 90% electron efficiency for momenta larger than 2 GeV/c is required.
The PHOS detector is a single-arm high-resolution electromagnetic calorimeter made with 17k lead tungstate crystals ($PbWO_4$) readout by silicon photodiodes designed to search for direct photons and to measure π^0 and η spectra at high momenta. It is located at 4.6 m from the vertex and covers 8 m^2. A charged-particle veto detector will be placed in front of the PHOS with the aim to identify charged particles reaching the calorimeter.
The forward muon arm is designed in order to cover the complete spectrum of heavy quark resonances up to the Υ family. It will measure the decay of these resonances into muons, both in proton-proton and in heavy-ion

collisions, with a mass resolution (about 100 MeV at quarkonia masses of 10 GeV) sufficient to separate all states. It consists of a complex arrangement of absorbers (reaching totally about 18 λ_{int}) to reduce as much as possible the punchthrough into the spectrometer and the backsplash into the TPC, a large dipole magnet (3 Tm integral field), ten stations of thin MWPC equipped with highly segmented cathodes for tracking and four Resistive Plate Chambers for muon identification and triggering.

8. Conclusions

Collisions between heavy nuclei represent a powerful tool to investigate the behaviour of nuclear matter at densities higher than the ground state density, where, according to the lattice-QCD calculations, a primordial non-hadronic bulk phase of strongly interacting matter will likely occur.
This plasma of quarks and gluons (QGP), within which colour freely propagates, being an ideal testing ground for fundamental concepts of QCD, requires an experimental insight. For this reason, a large community of physicists is engaged on such a very promising research located at the interface between particle and nuclear physics.
After the promising results achieved at CERN-SPS, new collider facilities (RHIC at BNL and LHC at CERN) will allow studying new signatures in view of their unprecedented energy in the centre-of-mass that will uniquely characterize the QGP and will allow the physicists to shed light and maybe draw conclusions on the character of the strong interaction.

Acknowledgements

I am very grateful to P. Dupieux and to the Director of the Joliot Curie School, C. Le Brun, for having invited me to give these lectures on the investigation of nuclear matter in extreme conditions of density and temperature. I hope that I succeeded to draw some of the students to study in depth such a challenging but fascinating subject.

References

1. T. Blum et al., Phys. Rev. D 51,5153 (1995).
2. R.C. Hwa, Quark-Gluon Plasma, Vol.1&2, Singapore : World Scientific.
3. C. Kuhn, "Plasma de quarks et de gluons et matière étrange du SPS au LHC", Joliot-Curie School 1998 – IReS 98-24.

4. J.W. Harris, Relativistic Heavy Ion Physics and the Relativistic Heavy ion Collider, Lake Louise Winter Institute on Quantum Chromodynamics, YRHI-98-13.
5. G.Baym, Nucl.Phys. A590 (1995) 233c-248c.
6. J.D. Bjorken, Phys. Rev. D27 (1983) 140.
7. T. Alber et al. (NA49 Collaboration), Phys. Rev. Lett. 75, 3814-3817 (1995).
8. M. Aggarwal et al. (WA98 Collaboration), Nucl. Phys. A610, 200c-212c (1996).
9. M. Murray et al. (NA44 Collaboration), Phys. Rev. Lett. 78, 2080 (1997).
10. R. Lietava et al. (WA97 Collaboration), J. Phys. G25, 181-188 (1999).
11. P. Braun-Munzinger, I. Heppe and J. Stachel, Phys. Lett. B465, 15-20 (1999).
12. L. D. Landau and E. M. Lifshitz, Statistical Physics (Addison-Wesley).
13. T. Matsui and H. Satz, Phys. Lett. B178 (1986) 416.
14. M.C. Abreu et al. (NA50 Collaboration), Phys. Lett. B 477, 28-36 (2000).
15. B. Lenkeit et al. (CERES Collaboration), Nucl. Phys. A661, 23c-32c (1999).
16. H. Appelshaeuser et al (NA49 Collaboration), Eur. Phys. J. C 2, 661-670 (1998).
17. M. Asakawa et al., Phys. Rev. Lett. 85 (2000) 2072.
18. F. Antinori et al., Nucl. Instr. and Meth. A360 (1995) 91.
19. A. Sandoval et al. (NA35 Collaboration), Nucl. Phys. A461 (1987) 465c-486c.
20. V. Eckardt et al., Nucl. Instr. and Meth. A315 (1992) 33.
21. HMPID TDR, CERN/LHCC 98-19.
22. A Transition Radiation Detector for Electron Identification within the ALICE Central Trigger - Addendum to the ALICE Technical Proposal, CERN/LHCC 99-13, May 1999.
23. http://www.bnl.gov/rhic/.
24. Conceptual Design Report for the Solenoidal Tracker At RHIC, The STAR Collaboration, PUB-5347 (1992); J. W. Harris et al., Nucl. Phys. A 566, 277c (1994).
25. PHENIX Experiment at RHIC – Preliminary Conceptual Design Report, PHENIX Collaboration Report (1992).
26. RHIC Letter of Intent to Study Very Low pt Phenomena at RHIC, PHOBOS Collaboration (1991).

27. Interim Design Report for the BRAHMS Experiment at RHIC, BNL Report (1994).
28. http://lhc.web.cern.ch/lhc/.
29. ALICE Technical Proposal, CERN/LHCC 95-71.